The Effects of Quantum Error Correction on Noisy Systems

by

Stefanie Beale

A thesis
presented to the University of Waterloo
in fulfillment of the
thesis requirement for the degree of
Master of Science
in
Physics (Quantum Information)

Waterloo, Ontario, Canada, 2018

This thesis consists of material all of which I authored or co-authored: see Statement of Contributions included in the thesis. This is a true copy of the thesis, including any required final revisions, as accepted by my examiners.

I understand that my thesis may be made electronically available to the public.

Statement of Contributions

1. Introduction

   - The plots in fig. 1.8 and the expressions for process matrices in noisy quantum error correcting codes when no recovery operations are applied (derived in section 1.8.3: *Noise on an Unencoded State*) and when a syndrome measurement is applied without a recovery operation (derived in section 1.8.3: *Noise on an Encoded State*) are new results, obtained by Stefanie Beale. Any other information in this section is either common knowledge or attributed to its source.

2. Chapter 2

   - The results presented in section 2.1-2.3 are the product of the collaborative effort of Stefanie Beale, Joel Wallman, Mauricio Gutiérrez, Kenneth R. Brown, and Raymond Laflamme. The project was initiated by Joel Wallman, Mauricio Gutiérrez, and Kenneth R. Brown; lemma 14 and theorem 16 were already derived before Stefanie Beale and Raymond Laflamme joined the project. The analysis of the scaling of noise at the logical level was developed by Stefanie Beale and Joel Wallman, and the discovery of theorem 18 followed a discussion with Raymond Laflamme.
   - The results of section 2.4 were a collaborative effort between Joel Wallman and Stefanie Beale.
   - The derivation in section 2.5 was undertaken by Joel Wallman and verified by Stefanie Beale. Stefanie Beale concluded that noise acting on fewer than d qubits in a distance d code would result in Pauli noise at the logical level.

3. Chapter 3

   - Theorem 21 and corollary 22 were derived by Joel Wallman. Stefanie Beale derived corollary 22 independently, and verified theorem 21.

- The results presented in section 3.1 resulted from a collaboration between Stefanie Beale and Joel Wallman. Joel Wallman found some of the permutation operators that generate symmetries; the remainder were acquired by a script written by Stefanie Beale.
- The results presented in section 3.2 are a product of collaboration between Stefanie Beale and Joel Wallman; the analysis in this section was guided by Joel Wallman while the execution was primarily carried out by Stefanie Beale.

Abstract

Full accuracy simulations of quantum systems are very costly, and as a result most studies of quantum error correction assume a probabilistic Pauli error model, largely because such errors can be efficiently simulated. Therefore, the behaviour of more general noise in a quantum error correcting code is poorly characterized. In this thesis, we present results which demonstrate the scaling of the logical noise with respect to the physical fidelity, and argue that the effective logical noise approaches a Pauli channel as the code distance increases, even when no recovery operations are applied. As a result, we argue that the average logical fidelity can be used to accurately quantify the effective logical noise, and to select recovery operations appropriate to the system. We further demonstrate that when physical noise acts on fewer than d qubits in an $[\![n, k, d]\!]$ code, the resultant noise is Pauli, and develop a method for approximating the dominant contributions to the effective logical noise up to a specified precision in terms of the physical infidelity. We derive conditions under which sets of recovery operations will produce equivalent logical noise channels, with examples of equivalencies in the 3 qubit repetition code, the 5 qubit code, the Steane code, and the Shor code. We also provide a general expression for the effective logical noise when the physical qubits undergo depolarizing or Pauli noise in a quantum error correcting code, examine the behaviour of depolarizing noise under concatenation of the 5 qubit and Steane codes, and present an algorithm for soft decoding which is not subject to statistical sampling, with an emphasis on the effective behaviour of a concatenated 5 qubit code undergoing depolarizing noise after applying a specialized version our soft decoding algorithm.

Acknowledgements

First and foremost, I would like to thank my supervisors, Raymond Laflamme and Joel Wallman, for their invaluable support and guidance throughout this degree; research is a collaborative effort, and without their input, these results would not exist. I would also like to thank Mauricio Gutiérrez and Kenneth R. Brown, with whom we collaborated for many of the results presented in the second chapter of this thesis. Thank-you to Steve Weiss for implementing a system for students such as myself to access computational resources at the IQC; your help was invaluable, and our discussions enlightening. The work presented in this thesis was funded in part by an NSERC CGS-M award and an Ontario Graduate Scholarship, by the University of Waterloo, and by the provincial and federal governments.

Thanks also to my thesis committee members, Roger Melko and Achim Kempf, and to Aimee Gunther, Morgan Mastrovich, Clifford Plesha, and many other friends and colleagues for their support and guidance during the writing of this document and before. Last, but certainly not least, I would like to thank my parents, Jo and Alan Beale, and my grandparents, Bill and Shirley Kilpatrick, without whom I would not be here.

Table of Contents

List of Tables

List of Figures

Nomenclature

$\mathbb{C}$	The set of codewords of a quantum error correcting code.
d	The code distance.
$\mathcal{D}$	A channel which decodes an encoded state.
$\mathcal{D}_p$	The process matrix for the depolarizing channel.
$\diamond(\mathcal{N})$	The diamond distance between $\mathcal{N}$ and the identity channel.
$\mathcal{C}$	A channel which encodes a logical state.
$\mathbb{G}$	The set of stabilizer generators for a quantum error correcting code.
g_i	The i^{th} stabilizer generator of a quantum error correcting code.
I	The 2×2 identity matrix.
k	The number of logical qubits in a quantum error correcting code.
m	An error syndrome: a binary vector of length $n-k$ giving the commutation relations of the error with the stabilizer generators.
m_0	The trivial error syndrome, $0^{\otimes(n-k)}$.
n	The number of physical qubits in a quantum error correcting code.
$\langle\overline{\mathcal{N}}_{\sigma,\sigma'}\rangle$	The (σ, σ') element of the effective logical process matrix corresponding to the physical noise $\mathcal{N}$ after full error correction has been applied, averaged over the set of recovery operations.
$\langle\overline{\mathcal{N}}_{\sigma,\sigma'}\rangle_{(\setminus R)}$	The (σ, σ') element of the effective logical noise channel after syndrome measurement, with no recovery operations applied, averaged over syndrome measurements.

$\overline{\mathcal{N}}(R_m)$ The logical process matrix resulting from encoding, exposing to noise $\mathcal{N}$, measuring a syndrome, m, applying a recovery operation, R_m, and decoding.

$\mathcal{N}$ A physical noise channel.

$\mathbb{P}$ The single qubit Pauli group, $\{I, X, Y, Z\}$.

Π_i Projective operators. When i is a syndrome, they project onto the eigenspace corresponding to that syndrome.

$\mathbb{P}_n$ The n-qubit Pauli group.

$\mathcal{R}_m$ A channel which measures the syndrome m syndrome and applies the associated recovery operation, R_m.

$r(\Phi)$ The average infidelity (where infidelity is defined as one minus the fidelity) of a channel, Φ, to the identity channel.

R_m The recovery operator associated with syndrome m in a quantum error correcting code.

$\mathcal{R}_x(\theta)$ The process matrix for the channel that applies a rotation about the x-axis by an angle θ.

$\mathcal{R}_z(\theta)$ The process matrix for the channel that applies a rotation about the z-axis by an angle θ.

$\mathcal{R}_{xyz}(\theta)$ The process matrix for the channel that applies a rotation about the axis equidistant from the x, y, and z axes by an angle θ.

$\mathcal{R}_y(\theta)$ The process matrix for the channel that applies a rotation about the y-axis by an angle θ.

$\overline{\sigma}$ A logical Pauli operator for a quantum error correcting code.

$\mathbb{S}$ The set of stabilizers for a quantum error correcting code.

X The Pauli matrix, σ_x.

$\mathcal{X}$ The process matrix for the channel that applies an X operation.

Y The Pauli matrix, σ_y.

$\mathcal{Y}$ The process matrix for the channel that applies a Y operation.

Z The Pauli matrix, σ_z.

$\mathcal{Z}$ The process matrix for the channel that applies a Z operation.

Chapter 1

Quantum Computation: What are we doing and how do we model it?

For the past several decades, technology has advanced rapidly, approximately following Moore's law, which states that the density of transistors that can be held on an integrated chip will double approximately every two years [1]. This rapid advancement has allowed computers to become an integral component of our society, driving research advancements in medicine, aeronautics, cosmology, and many other vital fields. Unfortunately, in recent years, this progress has slowed, and soon we will encounter a roadblock to the continuation of this technological evolution; if the size of transistors continues to decrease, quantum effects will come into play as transistors become progressively smaller and it will become impossible to continue to advance using solely classical technologies.

One shortcoming that is already present in traditional computation is that it is prohibitively expensive to simulate quantum systems with classical data. As such, it is difficult to design medications or simulate chemical reactions using classical computers. An alternative approach to simulating quantum systems was proposed by Richard Feynmann in 1982 [2]. Feynman suggested that a quantum computer, which would manipulate quantum data rather than classical data, could significantly outperform its traditional classical counterpart. The advent of quantum computing would additionally address the issue of quantum effects coming into play as Moore's law continues; quantum computers would themselves rely on these effects. Since 1982, quantum technologies have advanced significantly, and researchers worldwide are now racing to get as many quantum bits (qubits - see section 1.1) as possible on a myriad of platforms.

There are a few significant barriers to the successful implementation of a scalable quantum

computer. Among them, the high sensitivity of quantum systems to interactions with the surrounding environment; any interaction of the quantum system with the environment can introduce errors. In this thesis, we delve into methods for characterizing and treating errors in quantum systems. We begin this introductory chapter by reviewing quantum states and methods for describing their evolution. Then, we examine error correcting codes and the stabilizer formalism, before exploring methods for calculating and representing a noisy quantum channel.

1.1 Quantum States

The most common base element of quantum information used in quantum computing is a quantum bit, or qubit. A qubit is a two-level quantum system that can be used to store information. Alternatively, a d-level quantum system is referred to as a qudit. We define the computational basis for a single qubit, $\{|0\rangle, |1\rangle\}$,

$$|0\rangle = \begin{bmatrix} 1 \\ 0 \end{bmatrix} \text{ and } |1\rangle = \begin{bmatrix} 0 \\ 1 \end{bmatrix}, \tag{1.1}$$

The protocols introduced in this section for qubit systems can be trivially extended, e.g. by letting $|i\rangle = e_i$, where $\{e_i\}$ is the canonical basis, to span the space of a qudit. The $|0\rangle$ and $|1\rangle$ states typically correspond to a ground and excited state, respectively, in a physical system. An arbitrary pure single qubit state, $|\psi\rangle \in \mathbb{C}^2$, can be expressed in the computational basis as

$$|\psi\rangle = \alpha|0\rangle + \beta|1\rangle, \tag{1.2}$$

where $\alpha, \beta \in \mathbb{C}$ are referred to as probability amplitudes, and $|\alpha|^2$ and $|\beta|^2$ give the probability of measuring 0 and 1, respectively, when the state is projected onto the computational basis (see section 1.3). Alternatively, we can write a single qubit state in terms of a density matrix, ρ[1]. For a pure state, $\rho = |\psi\rangle\langle\psi|$, where $\langle\psi|$ is the conjugate transpose of $|\psi\rangle$. A mixed state is a probabilistic combination of pure states,

[1] In this thesis, we will follow the convention of referring to a state in $\psi \in \mathbb{C}^m$ (or $\rho \in \mathbb{C}^{m\times m}$) as an m-dimensional state.

$$\rho = \sum_k p_k |\psi_k\rangle\langle\psi_k|. \tag{1.3}$$

An arbitrary single-qubit state can be expressed in the form of a density matrix as a linear combination of basis elements of hermitian matrices in $\mathbb{C}^{2\times 2}$. An n-qubit state can be expressed as a density matrix in $\mathbb{C}^{2n\times 2n}$.

1.2 Quantum Channels

The evolution of quantum states is described by quantum channels. A state can evolve via deliberate operations or from the effects of noise introduced by poorly implemented operations or interaction with its surroundings.

Definition 1. A quantum channel is a completely positive and trace-preserving (CPTP) linear map that maps quantum states to quantum states.

An arbitrary linear map, Φ, acting on a matrix, ρ, can be described in the Kraus formalism as follows[2]

$$\Phi[\rho] = \sum_k A_k \rho K_k^\dagger \tag{1.4}$$

where $\{A_k\}$ and $\{K_k\}$ are known as Kraus operators. If Φ is completely positive, $A_k = K_k$ $\forall k$. So for all quantum channels (hereafter channels), $A_k = K_k \forall k$. The selection of Kraus operators is non-unique for a given map.

1.2.1 Common Errors and Operations on Quantum States

Classical Errors

In classical systems, after a system is sampled from an analog to a digital signal, the net effect of any errors will be that some bits flip (that is, some desired 0s will appear as 1s and vice versa); the exact mechanisms for data processing in classical systems will not be explored in this thesis.

[2] Throughout this document, when a channel acts on a state, the state will be enclosed in square braces. When a channel depends on some parameter(s), the parameter(s) will be enclosed in round braces.

Quantum Errors

In quantum systems, states are more complex and thus, single bit errors can take a much more complicated form. Let $|\phi\rangle = \alpha|0\rangle + \beta|1\rangle$. The quantum analog of a bit flip operator is denoted by X, and maps

$$|\phi\rangle \to \alpha|1\rangle + \beta|0\rangle, \tag{1.5}$$

or, equivalently, $X|\phi\rangle = \alpha|1\rangle + \beta|0\rangle$, where X is the Pauli matrix

$$X = \begin{bmatrix} 0 & 1 \\ 1 & 0 \end{bmatrix}. \tag{1.6}$$

Quantum systems can also undergo phase flips, which map

$$|\phi\rangle \to \alpha|0\rangle - \beta|1\rangle. \tag{1.7}$$

Phase flips are denoted Z, and the combination of a bit flip error and phase flip error is written $Y = iXZ$, where Z and Y are Pauli matrices,

$$Z = \begin{bmatrix} 1 & 0 \\ 0 & -1 \end{bmatrix} \qquad\qquad Y = \begin{bmatrix} 0 & -i \\ i & 0 \end{bmatrix}. \tag{1.8}$$

Together with the identity matrix, I, the Pauli matrices form a complete basis over hermitian matrices in $\mathbb{C}^{2\times 2}$, so that any single qubit operation or error can be represented as a linear combination of these matrices. We define the single qubit Pauli group, $\mathbb{P} = \{I, X, Y, Z\}$, and the n-qubit Pauli group, $\mathbb{P}_n = \{I, X, Y, Z\}^{\otimes n}$.

The evolution of a quantum system can be described by unitary operations, ie operations, U, for which $U^\dagger U = I$.

The n-qubit Clifford group, $\mathbb{C}_n$, is a special case of unitary operations that maps non-identity Pauli operators to non-identity Pauli operators,

$$\mathbb{C}_n = \{U \in U(2^n) | U\sigma U^\dagger \in \pm\mathbb{P}_n \backslash I^{\otimes n} \; \forall \sigma \in \pm\mathbb{P}_n \backslash I^{\otimes n}\}/U(1). \tag{1.9}$$

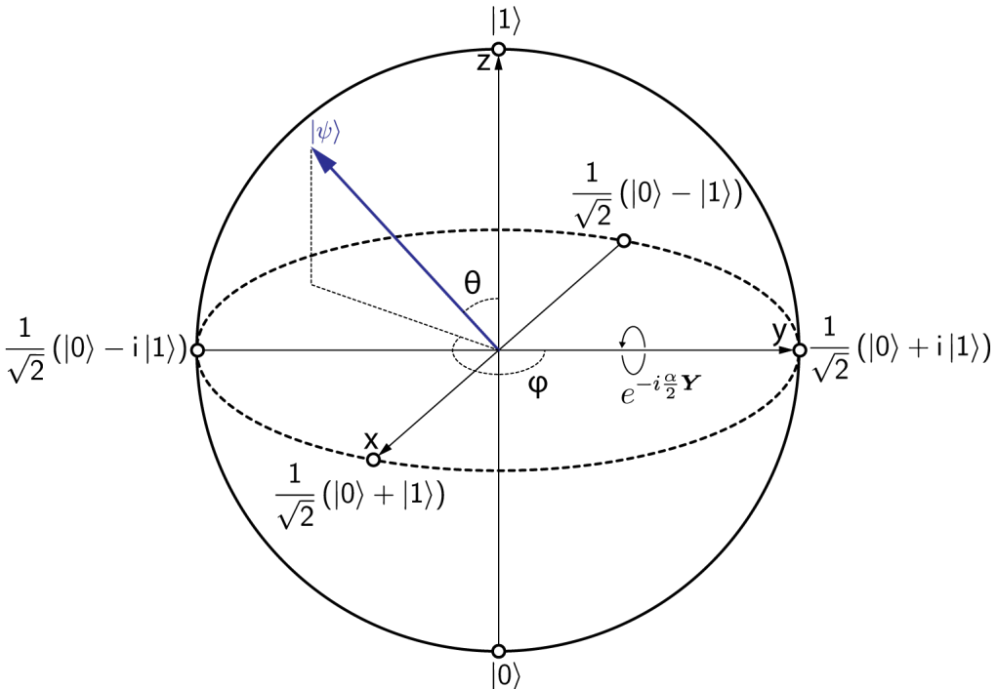

Figure 1.1: The Bloch sphere [3]. A pictoral representation of the state space of a single qubit. Unitary operations are represented as rotations of the Bloch sphere; a quantum state is represented as a unit vector.

Modeling Quantum Error Channels

This section describes some common sources of errors in quantum systems, as well as the theory used to describe them. These concepts are integral to understanding how best to leverage a noisy quantum system, including how to correct errors effectively.

Definition 2. A unitary channel is a channel whose action on a density matrix, ρ, can be written $\Phi[\rho] = U\rho U^\dagger$, for some unitary operator, U.

A unitary operation can be imagined as a rotation of the state space. It is often convenient to picture the state space as a unit sphere construct called the Bloch sphere, pictured in fig. 1.1.

Operations on quantum states are often referred to as gates. One common source of error is over or under-rotation when gates are applied. This is generally modeled by a unitary rotation channel, which can be expressed as single Kraus operator given by $e^{i\theta\vec{n}\cdot\vec{\sigma}}$, where $\vec{n}$ is a vector with $\vec{n}^\dagger \cdot \vec{n} = 1$, $\vec{\sigma} = (X, Y, Z)$, and

$$e^{i\theta\vec{n}\cdot\vec{\sigma}} = \cos\theta I + i\sin\theta(\vec{n}\cdot\vec{\sigma}). \tag{1.10}$$

Definition 3. A mixed unitary channel, Φ, is a channel that can be expressed as a convex combination of unitary channels as follows

$$\Phi[\rho] = \sum_k p(k) U_k \rho U_k^\dagger, \tag{1.11}$$

where p is a probability vector, $0 \leq p(k) \leq 1 \, \forall k$ and $\sum_k p(k) = 1$.

Definition 4. A Pauli channel is a mixed unitary channel with $U_k \in \mathbb{P} \, \forall k$.

Pauli channels are useful because they are easy to simulate and, because the Pauli matrices form a complete basis over Hermitian matrices in $\mathbb{C}^{2\times 2}$, a code can correct an arbitrary single-qubit error if and only if at can correct any single qubit Pauli error.

Definition 5. A channel, Φ, is unital if $\Phi[I] = I$.

Unitary and mixed unitary channels are unital. A metric was introduced in [4] to quantify how close a channel is to unitary; the unitarity, $u(\Phi)$, of a channel, Φ, is defined as

$$u(\Phi) = \frac{d}{d-1} \int \mathrm{Tr}(\Phi'[\psi]^\dagger \Phi'[\psi]) d\psi, \tag{1.12}$$

where the integral is over all pure states, and Φ' is defined such that $\Phi'[I] = 0$ and $\Phi'[A] = \Phi[A] - \frac{\mathrm{Tr}(\Phi[A])}{\sqrt{d}} I$ for traceless A. Then, because an arbitrary matrix M can be expressed as $cI + A$ for some constant c and traceless matrix A, by linearity $\Phi'[M] = c\Phi'[I] + \Phi'[A] = \Phi'[A]$.

Not all channels are Pauli channels. A common non-Pauli source of error in physical systems is the decay of an excited state to the ground state. This is modeled by an amplitude damping channel, in which an excited state decays from $|1\rangle$ to $|0\rangle$ with some probability, p, while the ground state, $|0\rangle$, remains unchanged. The amplitude damping channel can be described by the Kraus operators, $\{A_i\}$, in eq. (1.13). The amplitude damping channel is neither mixed unitary nor unital.

$$A_0 = \begin{bmatrix} 0 & \sqrt{p} \\ 0 & 0 \end{bmatrix} \text{ and } A_1 = \begin{bmatrix} 1 & 0 \\ 0 & \sqrt{1-p} \end{bmatrix}. \tag{1.13}$$

It is possible to achieve a Pauli approximation of a channel via a process referred to as Pauli twirling [5]. This is achieved by taking the average result of conjugating a channel with Pauli operators. More generally, twirling is the process of taking the average channel under conjugation by a set of unitaries. Pauli twirling is achievable experimentally and is easily achieved in simulations and theory [5].

The completely depolarizing channel is a common example of a Pauli channel used to model noise; it describes a process in which the input state is replaced with the maximally mixed state with probability p, and left unchanged with probability $1-p$. The completely depolarizing channel can be described by the Kraus operators $A_0 = \sqrt{1-3p/4}I$, $A_1 = \sqrt{p/4}X$, $A_2 = \sqrt{p/4}Y$, and $A_3 = \sqrt{p/4}Z$.

Definition 6. An operator has weight w if it acts non-trivially on w qubits.

1.2.2 Other Common Operations on Quantum Channels

This section introduces two common 2-qubit operations used in quantum computing, as well as the single-qubit Hadamard operator. The first 2-qubit gate is the controlled-NOT (CNOT) gate. The CNOT gate applies an X gate to one qubit when the other qubit is in the excited state, and does nothing otherwise. The qubit which determines whether X is applied is called the control qubit, and the qubit acted upon is the target qubit. The operator for a CNOT gate is

$$\text{CNOT} = \begin{bmatrix} 1 & 0 & 0 & 0 \\ 0 & 1 & 0 & 0 \\ 0 & 0 & 0 & 1 \\ 0 & 0 & 1 & 0 \end{bmatrix}. \tag{1.14}$$

Another operation that is commonly used in quantum computing is the SWAP gate, which exchanges the position of two qubits. The SWAP gate is

$$\text{SWAP} = \begin{bmatrix} 1 & 0 & 0 & 0 \\ 0 & 0 & 1 & 0 \\ 0 & 1 & 0 & 0 \\ 0 & 0 & 0 & 1 \end{bmatrix}. \tag{1.15}$$

Later, in chapter 3, we will use cyclic permutation operators, which are operations that apply many SWAP gates to permute qubits. For notational convenience, we use the notation of group theory for these operations. Cyclic permutations are denoted by a series of numbers grouped into brackets; the numbers index which qubit is mapped to which position. In each bracket, every number is the index of a qubit being mapped and the number to its right is the index it should be mapped to, with the rightmost number in a bracket mapping to the leftmost number's position. For example, the operator $(134)(25)$ writes the first qubit to the third position, the third qubit to the fourth position, the fourth qubit to the first position, the second qubit to the fifth position, and the fifth qubit to the second position.

The single-qubit Hadamard transform is a gate which maps $X \leftrightarrow Z$, and is given by

$$H = \frac{1}{\sqrt{2}} \begin{bmatrix} 1 & 1 \\ 1 & -1 \end{bmatrix}. \tag{1.16}$$

1.3 Measurement

Meauring a quantum state, $|\psi\rangle = \alpha|0\rangle + \beta|1\rangle$, in the computational basis will collapse the wavefunction to classical states 0 or 1[3] with probability $|\alpha|^2$ or $|\beta|^2$, respectively. Because we generally want to continue using an encoded quantum state after applying error correction protocols, it is imperative that we avoid collapsing to a classical state. To garner information about a state without destroying it, we instead use a class of measurements called projective measurements, which project the state onto an eigenspace of the measured operator. This section describes the action of projective measurements and the information that is retrieved by applying these operations.

When we apply a projective measurement, we say that we are measuring some operator, Λ, which can be decomposed as

$$\Lambda = \sum_i \lambda_i \Pi_i, \tag{1.17}$$

where $\{\lambda_i\}$ are the eigenvalues of Λ and Π_i is a projector onto the eigenspace of Λ corresponding to λ_i. If we measure Λ on some state, $|\psi\rangle$, the resultant state will be in the

[3] The classical states 0 and 1 are states in the computational basis of a qubit; for an m-dimensional state, the computational basis states would be $\mathbb{Z}_m$.

eigenspace corresponding to λ_i with probability $\langle\psi|\Pi_i|\psi\rangle$, and the state after measurement is

$$\frac{\Pi_i|\psi\rangle}{\sqrt{\langle\psi|\Pi_i|\psi\rangle}}. \tag{1.18}$$

Measurements are typically applied using qubits outside of the state being measured[4]. Note that through the measurement process, we can learn which eigenspace the state was projected onto.

1.4 Circuit Representation

It is often convenient to represent quantum channels pictorally. This is achieved through the use of quantum circuit diagrams, in which qudits are denoted by horizontal lines and gates as images overlaid over the qudits. Figure 1.2 shows a basic example of a quantum circuit.

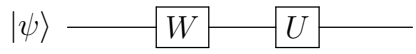

Figure 1.2: Basic example of a quantum circuit diagram in which a W operator is applied to the state $|\psi\rangle$, followed by a U operator. Time flows from left to right by convention.

Multi-qudit operations are represented by images overlaid over multiple qudits in a circuit, as demonstrated in fig. 1.3. A multi-qudit gate is expressed as an operator in a larger space. If it acts on each qubit individually, it can be broken down as a tensor product of single qubit operators. Throughout this thesis, when we examine multi-qudit operators that act in this manner, we will omit the tensor product symbol for notational simplicity.

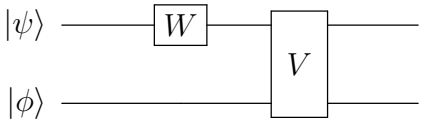

Figure 1.3: Basic example of a multi-qudit quantum circuit diagram in which a single qudit gate, W, acts on $|\psi\rangle$, followed by a multi-qudit gate, V, which acts on $W|\psi\rangle$ and $|\phi\rangle$.

[4] This process will become apparent in section 1.5.

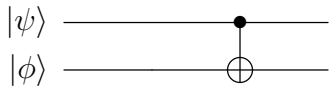

Figure 1.4: The circuit representation of a quantum CNOT gate, where ψ is the control qubit, and ϕ is the target. A controlled gate with a different action on the target qubit is represented by a similar symbol in which the circle on the target qubit is replaced by the symbol representing the desired operation.

Measurement in the computational basis is represented in a quantum circuit by the symbol shown in fig. 1.5. It is worth noting that there is no qudit exiting the gate on the right because measurement destroys the state.

Figure 1.5: Quantum circuit diagram representation of a measurement operation.

In the case of encoded qudits, it is often convenient to denote a single logical qudit, which is encompassed by many physical qudits (see section 1.5), as a single horizontal line in a quantum circuit diagram.

1.5 Error Correcting Codes

Errors are introduced into quantum systems when the system is not sufficiently isolated from the surrounding environment and when gates are not perfectly implemented. To correct these errors, it is necessary to use some sort of quantum error correcting protocol. This section reviews the basics of quantum error correcting codes.

1.5.1 Classical Repetition Code

In classical computing, states are often protected from errors by encoding in a repetition code, that is, by copying every bit of data onto additional "ancilla" bits to create redundancy. We denote encoded (logical) bits by a bar, so a three bit encoding for a classical repetition code would be expressed as

$$0 \to \overline{0} = 000 \tag{1.19}$$

$$1 \to \overline{1} = 111. \tag{1.20}$$

For example, the string "010" would be encoded as "000111000".

Errors are then corrected by measuring every physical bit in each logical bit and flipping any bit that doesn't agree with the majority. Introducing a bit flip error on the second last physical bit in the above example, we have "000111010". When we measure the third logical bit, we see that the second physical bit doesn't match the others and will accurately correct the error. If, however, two single bit errors were introduced in the same logical bit, e.g. "000111011", we would attempt to correct the wrong error so that the end result would be "000111111", thus introducing a logical fault, as this would then be decoded as "011" rather than the intended "010". However, this recovery method works the majority of the time because the error rate in classical systems is incredibly small [6][5].

1.5.2 Quantum Repetition Code

The classical error correction methods described in section 1.5.1 are not possible in quantum systems because, by the no-cloning theorem [7], quantum states cannot be copied, so the classical encoding cannot be replicated for a logical quantum state. Further, measuring a quantum state destroys it, so observing the state to see errors directly is not possible, and errors are continuous, unlike errors in digitized classical data.

In quantum computing, encoding creates redundancy in a similar way; data is protected using additional ancilla qubits, albeit in a different manner. Ancilla qubits are also used to get information about errors in quantum error correcting codes.

Definition 7. The set of codewords, $\mathbb{C}$, of a quantum error correcting code is the set of encoded computational basis states.

The quantum repetition code is constructed by defining logical states $|\overline{0}\rangle = |000\rangle$ and $|\overline{1}\rangle = |111\rangle$. This encoding does not violate the no-cloning theorem because a general state $|\psi\rangle = \alpha\,|0\rangle + \beta\,|1\rangle$ maps to $|\overline{\psi}\rangle = \alpha\,|\overline{0}\rangle + \beta\,|\overline{1}\rangle$, rather than $(\alpha\,|0\rangle + \beta\,|1\rangle)^{\otimes 3}$ and so the state is not copied in the encoding process. The encoding circuit for the 3 qubit repetition code is given in fig. 1.6.

[5] This study reported one memory error on average in 41 hours on a node with 4GB of DRAM with no error correction in 2016.

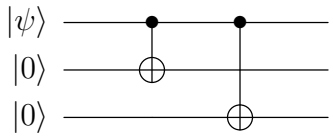

Figure 1.6: Encoding circuit for the quantum repetition code.

To detect bit flip errors on states encoded in the quantum repetition code, we can detect differences between any two pairs of physical qubits without directly measuring the encoded state as shown in fig. 1.7.

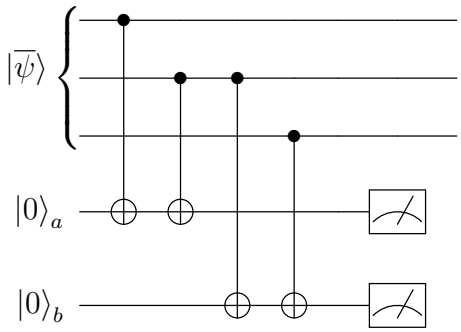

Figure 1.7: Measuring bit flip errors on the 3 qubit repetition code.

Measuring ancilla qubits a and b tells us whether the first and second qubit and second and third qubit in the encoded state match, respectively. The outcome of these measurements is a two bit string called a measurement syndrome, which provides insight into what errors might have occurred. Assuming that bit flip errors are the only source of noise in our system, we can try to correct the noise based on the measured error syndrome. Error syndromes and the associated bit flip errors are listed in table 1.1.

Label	a	b	Errors
m_0	0	0	$\underline{I^{\otimes 3}}$, $X^{\otimes 3}$
m_1	0	1	$\underline{IIX}$, XXI
m_2	1	0	$\underline{XII}$, IXX
m_3	1	1	$\underline{IXI}$, XIX

Table 1.1: Syndromes and corresponding bit flip errors for the 3 bit repetition code.

Assuming a low probability of error (in a useful quantum system, this is a reasonable assumption), we generally choose to correct the underlined error associated with each syndrome in table 1.1; if each qubit has a low probability p of undergoing a bit flip error, then

the underlined errors are significantly more likely to occur than the others. Correcting an error that did not occur can result in a logical error. For example, if an XXI error occurs and we measure the correct syndrome, $(0, 1)$, but we assume that IIX has occurred and apply IIX as a correction, we will then have the encoded state acted upon by XXX, thus producing a logical fault[6].

The indistinguishability of these errors is symptomatic of a pervasive issue in quantum error correction; the only information available to try to correct errors in a quantum error correcting code is which syndrome was measured, which could correspond to many different errors. This difficulty is well summarized by the Knill-Laflamme conditions for error correction, presented in ref. [8], which give necessary and sufficient conditions for a state to be recoverable after it has undergone some noise process.

The codewords of a code form an orthonormal basis of the codespace. In terms of the codewords, $\{|\overline{\psi}_i\rangle\} \in \mathbb{C}$, the first Knill-Laflamme condition for the correctability of two errors, E and F, is as follows:

1. $\langle\overline{\psi}_i|E^\dagger F|\overline{\psi}_i\rangle = \langle\overline{\psi}_j|E^\dagger F|\overline{\psi}_j\rangle$
2. $\langle\overline{\psi}_i|E^\dagger F|\overline{\psi}_j\rangle = 0.$

It should be noted that this condition applies for any orthonormal basis of the codespace, rather than just the set of codewords. The other conditions presented in [8] are equivalent and we restrict attention to this one for brevity.

We can construct a similar code which corrects phase errors by replacing the CNOT gates in fig. 1.6 with controlled-Z gates and applying Hadamard gates to the ancilla qubits before and after the CNOTs in the syndrome measurement.

1.5.3 Stabilizer Codes and their Error Correction Protocols

In this section, we discuss a particular class of quantum error correcting codes known as stabilizer codes. The quantum repetition code introduced in the previous section is an example of a stabilizer code.

A stabilizer code is a quantum error correcting code (QECC) that is described by operators which stabilize the logical (i.e encoded) computational basis states. That is, operators, S, for which

[6] Applying the recovery operator introduces a logical fault because it maps $|\overline{0}\rangle \leftrightarrow |\overline{1}\rangle$.

$$S|\bar{l}\rangle = |\bar{l}\rangle,\ \forall l \in \mathbb{Z}_q, \tag{1.21}$$

where q is the dimension of the logical state.

Definition 8. The codespace of a quantum error correcting code is the space spanned by the $+1$ eigenstates of the code, that is, the set of encoded logical states.

Definition 9. The set of operators, $\mathbb{S}$, which stabilize the codewords is the stabilizer group

The stabilizer group has size $|\mathbb{S}| = 2^{n-k}$ for a QECC which encodes k logical qubits in n physical qubits.

Definition 10. The minimal generating set for the stabilizer group are the stabilizer generators[7], $\mathbb{G}$.

The group of stabilizer generators for a code which encodes k logical qubits in n physical qubits has size $|\mathbb{G}| = n-k$. A stabilizer code is generally specified by its stabilizer generators.

For a given stabilizer code, we define a set of "logical" Pauli operators, $\{\overline{\sigma}\} \in \pm\mathbb{P}_n$. Recall that $\mathbb{P}_n = \{I, X, Y, Z\}^{\otimes n}$ is the n-qubit Pauli group. The logical Pauli operators act on the encoded state as the Pauli operators would act on the unencoded state. These operators have the same commutation relations as the unencoded Paulis, and commute with every element of the stabilizer group, $\mathbb{S}$.

Definition 11. The normalizer, $\mathbb{N}(\mathbb{S})$, of a quantum error correcting code is the set of Pauli operators that commute with every element of that stabilizer group. That is, $\mathbb{N}(\mathbb{S}) = \{M \in \{\pm 1, \pm i\}\mathbb{P}_n : [M, S] = 0 \forall S \in \mathbb{S}\}$.

Definition 12. A cospace of a quantum error correcting code is the image of the codespace under a coset of the normalizer in $\{\pm 1, \pm i\}\mathbb{P}_n$.

The quantum repetition code discussed in section 1.5.2 is an example of a stabilizer code, with stabilizer generators ZZI, and IZZ. Figure 1.7 shows these generators being measured, and the resultant measurement outcomes[8] gives the commutation relations of the stabilizer generators with the error that has occurred.

[7] The stabilizer generators of a code are often referred to as simply the generators of that code.

[8] The resultant measurement outcome is the measured syndrome.

More generally, after some noise process is applied to the encoded state in an arbitrary stabilizer code, projective measurements, Π_m, are applied, mapping the state onto a cospace of the code associated with syndrome measurement m, where m is a binary vector of length $n-k$; each bit of m is specified by the commutation relation of a generator with the error that has occurred. So, after an error, e, the i^{th} bit of m is decided by the commutation relation between the i^{th} generator, g_i and e. So $m(i) = 0$ when $[e, g_i] = 0$ and $m(i) = 1$ when $\{e, g_i\} = 0$. The trivial syndrome, $0^{\otimes(n-k)}$, is denoted m_0.

A projection operator onto the ± 1 eigenspace of a generator, g_i, can be written $(I^{\otimes(n-k)} \pm g_i)/2$. The projection operators, Π_m, used to project onto the cospace associated with syndrome m, and consequently measure syndrome m, can then be expressed as a product of measurements of the individual generators,

$$\Pi_m = \prod_j (I^{\otimes n} + (-1)^{m(j)} g_j), \tag{1.22}$$

where g_j is the j^{th} stabilizer generator, and $m(j)$ is the j^{th} bit of m.

After syndrome measurement, a recovery operation, R_m, associated with the cospace is then applied to map the state back to the codespace. The selection of effective recovery operations is imperative to the successful implementation of an error correcting code; as discussed in section 1.5.2, selecting suboptimal recovery operations can introduce logical faults. This problem is discussed in detail in section 1.6, and the results presented in this thesis underscore the efficacy of a particular method of selecting recovery operations (see section 2.3).

The notion of code distance in quantum error correction is analogous to that used in classical error correcting codes, and there are many equivalent definitions. We will use the definition provided below herein.

Definition 13. The distance of a quantum error correcting code is the minimum weight of an operator which maps one codeword to another.

A QECC which encodes k logical qubits in n physical qubits and has distance d is denoted as an $[\![n, k, d]\!]$ code. An $[\![n, k, d]\!]$ code can correct the set of t-qubit errors, where $t \leq \lfloor (d-1)/2 \rfloor$ [9].

QECCs are often used in concatenation schemes to increase code distance. This is accomplished by re-encoding each physical qubit in an encoding with another (or the same)

QECC, recursively. Re-encoding with the same QECC at each level of concatenation is often used to find thresholds for the performance of a given QECC [10–12]. This thesis does not address fault tolerance, however it is worth noting that concatenating using different QECCs has been used to get a universal set of fault-tolerant gates on the full encoded state [13].

1.5.4 Popular Examples of Stabilizer Codes

One of the more popular quantum error correction codes is the $[\![5, 1, 3]\!]$ code. The stabilizer generators of the 5 qubit code are given in table 1.2. This code is referred to as a "perfect" code because each single qubit Pauli error (plus the trivial error) is associated with a unique syndrome and there are no syndromes leftover.

X	Z	Z	X	I
I	X	Z	Z	X
X	I	X	Z	Z
Z	X	I	X	Z

Table 1.2: Stabilizer generators for the $[\![5, 1, 3]\!]$ code.

The 9-qubit Shor code is created by concatenating the 3 qubit repetition (bit flip) code and the 3 qubit phase flip code to form a code which can correct all single qubit bit flip or phase flip errors. The Shor code is specified by the generators given in table 1.3.

Z	Z	I	I	I	I	I	I	I
I	Z	Z	I	I	I	I	I	I
I	I	I	Z	Z	I	I	I	I
I	I	I	I	Z	Z	I	I	I
I	I	I	I	I	I	Z	Z	I
I	I	I	I	I	I	I	Z	Z
X	X	X	X	X	X	I	I	I
I	I	I	X	X	X	X	X	X

Table 1.3: Stabilizer generators for the 9 qubit Shor code.

Calderbank-Steane-Shor (CSS) codes are created by mapping the parity check matrix of

classical codes[9] to Pauli operators as follows: half of the stabilizer generators are constructed by taking each row of the parity check matrix for a classical code and replacing every 0 with I and every 1 with X. To construct the remaining stabilizer generators, this process is repeated, using a code that is the dual of the first code, but with $0 \to I$ and $1 \to Z$. The Steane code is an example of a CSS code, and is constructed from the classical 7 bit Hamming code, with stabilizer generators given in table 1.4. There are many other CSS codes; the $[\![15, 1, 3]\!]$ Reed-Muller is one of the more popular examples, and one of the larger codes commonly studied.

Z	Z	Z	Z	I	I	I
Z	Z	I	I	Z	Z	I
Z	I	Z	I	Z	I	Z
X	X	X	X	I	I	I
X	X	I	I	X	X	I
X	I	X	I	X	I	X

Table 1.4: Stabilizer generators for the 7 qubit Steane code.

1.6 The Decoder Problem

The outcome of a syndrome measurement tells us the commutation relation of each generator with the error that has occurred, but because this is the only information available about the error and many errors could have the same commutation relations, there is some uncertainty as to which error has actually acted on the encoded state. As discussed in section 1.5.2, correcting the wrong error can introduce a logical fault, so selecting an appropriate recovery operation to associate with the corresponding syndrome is crucial. In this section, we discuss some approaches for selecting recovery operations.

In any protocol for the selection of recovery operations, it is necessary to have a method for approximating the noise acting on a quantum channel. For example, if we know that the most common errors afflicting a channel are bit flips, and other types of errors are rare, selecting recovery operations which have non-zero weight on only X operators wherever possible follows logically. Alternatively, if we know nothing about the noise acting on a channel, the default is generally to select the lowest weight error associated with every

[9] We omit an introduction to classical error correcting codes for brevity; for a thorough introduction, see [14].

syndrome because for a successful implementation, the probability of a physical error must be low, and if the probability of an error on a single qubit is p, then the probability of that error occurring on a given pair of qubits is[10] $p^2 \leq p$. When an error with the lowest possible weight is associated with each syndrome measurement, the recovery protocol is called symmetric recovery. It is common for theoreticians to assume a particular noise channel to model the effects of selecting different recovery operations, but a full density matrix simulation for a channel is costly, particularly in a code with large distance (or a concatenated code).

For ease of simulation, it is common for researchers to assume Pauli noise, and restrict to simulating only a few levels of concatenation or low distance encodings. This assumption has been accepted by the research community because logical noise is believed to converge to Pauli noise as code distance increases. However, even with the restriction to Pauli noise, simulation is costly, leading to simulation methods ranging from using tensor networks [11] to machine learning [15].

Further difficulty arises when we go beyond a single level of concatenation and need to select recovery operations at several levels, leading to the possibility that the best set of recovery operations will make the noise worse at one level only to improve it at a higher level. Searching for the optimal set of recovery operations over all levels of concatenation is computationally costly. As a result, many studies of concatenated codes restrict attention to "hard" decoding protocols, where recovery operations are selected for optimal performance independently at each level of concatenation. Some "soft" decoding algorithms have been explored, where recovery operations are selected using knowledge of the recovery operations chosen at other levels of concatenation [12, 16].

To evaluate the performance of a set of recovery operations, it is necessary to have some metric with which to quantify the severity of the errors resulting from applying a given set. Section 1.7 discusses methods for quantifying errors. In [10], we proposed an algorithm which uses the average logical infidelity[11] to select recovery operations.

1.6.1 An Example: Selecting Recovery Operations for the $[\![5, 1, 3]\!]$ Code

As discussed in section 1.6, the selection of recovery operations can drastically alter the performance of a quantum error correction code under a given noise model. In this section,

[10] For each syndrome measurement outcome, we can only choose to correct a single 2-qubit error or a single 1-qubit error. The number of each type that could occur is therefore irrelevant.

[11] Which we define as one minus the average logical fidelity (see section 1.7).

we explore the selection of recovery operations for the $[\![5, 1, 3]\!]$ code under different noise models to demonstrate this variance.

It is possible to associate every single-qubit Pauli error (including the trivial error) with a unique syndrome in the $[\![5, 1, 3]\!]$ encoding. It is also possible to associate every error in the set containing single-qubit Z errors and two qubit Z errors as well as the trivial error with unique syndromes. The effect of selecting one of these decoders versus the other[12] varies based on the noise present in the system. This is illustrated by the example in fig. 1.8, which plots the average logical infidelity (a metric[13] for measuring error rate - see section 1.7) against the angle of rotation for channels undergoing coherent rotations about different axes for the two sets of recovery operations described above.

[12] Or selecting any alternate decoder.

[13] Note that in this document the word metric is used in a non-technical sense as a synonym for "figure of merit;" infidelity is a semimetric as it does not satisfy the triangle inequality.

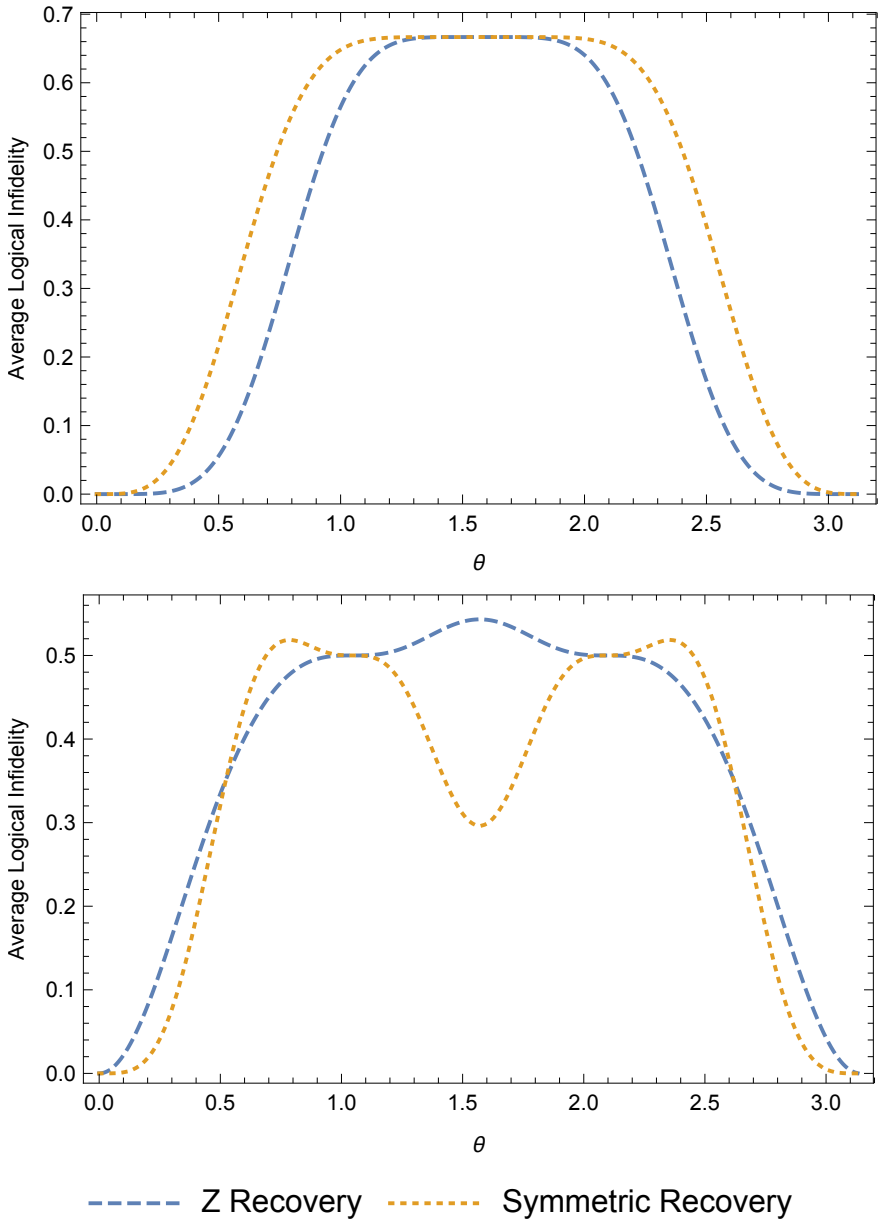

Figure 1.8: Plots of the average logical infidelity under Z recovery and symmetric recovery for a coherent rotation about the Z axis (top) and a coherent rotation about an equally weighted axis[14](bottom).

If we have a rotation about an axis equally weighted in X, Y, and Z, then selecting the lowest weight recovery operations will be more effective for low angles than applying strictly

[14] A unitary rotation as defined in section 1.2.1 with $\vec{n} = (1/\sqrt{3}, 1/\sqrt{3}, 1/\sqrt{3})$.

Z recovery operations. Alternatively, if we have a rotation about the Z axis, it is better to apply recovery operations with non-zero weight only on Z operators for a rotation by any angle. In useful quantum systems, we should have small θ.

1.7 Quantifying Errors

In any computation, it is important to have some metric which quantifies the reliability of the result; several methods have been developed to analyse the severity of noise in quantum systems.

Some specific noise channels have a form that lends itself easily to defining an error rate. A Pauli channel, for example, has some probability of applying a non-identity operation; that probability could easily be viewed as the error rate for that channel. For a channel which applies a unitary rotation, by contrast, it is not immediately obvious what metric should be used to quantify the severity of the error. Further, the probability of error has no clear analog at the logical level.

The average gate infidelity[15] to the identity (hereafter infidelity) is one metric developed to quantify error rate in quantum systems. It is the most commonly used metric by experimentalists because it can be estimated efficiently in physical systems via randomized benchmarking (see ref. [17]). The infidelity, $r(\Phi)$, of a channel Φ, to the identity channel is given by eq. (1.23).

$$r(\Phi) = 1 - \int \langle\psi|\Phi(|\psi\rangle\langle\psi|)|\psi\rangle d\psi, \tag{1.23}$$

where the integration is over the uniform Haar measure on pure states. In terms of the Kraus operators, $\{A_k\}$, of the channel, Φ, the infidelity is[16] [5, 18]

$$r(\Phi) = \frac{\sum_k |\mathrm{Tr}(A_k)|^2 + q}{q(q+2)}. \tag{1.24}$$

The diamond distance, $\diamond(\cdot)$, is another common metric for error quantification, and is commonly used by theoreticians as a worst-case error analysis. It is defined relative to the identity channel, $\mathcal{I}$, by eq. (1.25),

[15] We define infidelity as one minus the fidelity.

[16] In the interest of brevity, we omit the details of this derivation.

$$\diamond(\Phi) = \sup_{\psi} \frac{1}{2} \|(\Phi \otimes \mathcal{I}_m - \mathcal{I}_{m^2})(\psi)\|_1, \tag{1.25}$$

where the supremum is over all q^2-dimensional pure states to account for the effect of the channel on an entangled state.

The diamond distance is related to the infidelity by [19, 20]

$$\frac{q+1}{q} r(\Phi) \leq \diamond(\Phi) \leq \sqrt{q(q+1)} \sqrt{r(\Phi)}, \tag{1.26}$$

with

$$\diamond(\mathcal{P}) = \frac{q+1}{q} r(\mathcal{P}) \tag{1.27}$$

for Pauli noise $\mathcal{P}$ [21]. For unitary rotations, $\mathcal{U}$, $\diamond(\mathcal{U})$ is proportional to $\sqrt{r(\mathcal{U})}$, but does not necessarily saturate the upper bound in eq. (1.26)[22].

Both the fidelity and diamond distance metrics extend easily to characterizing the severity of logical errors. However, comparing physical and logical error rates with these two metrics demonstrates some significant discrepancies in their characterization; the diamond distance and fidelity often differ by orders of magnitude when describing the effects of the same noise channel. Figure 1.9 shows results from [23] comparing physical diamond distance and physical fidelity to logical fidelity for randomly generated CPTP maps. Notice that the plots highlight that the depolarizing (Z rotation) noise has the best logical fidelity when compared to the physical diamond distance (fidelity), and the worst logical fidelity when compared to the physical fidelity (diamond distance).

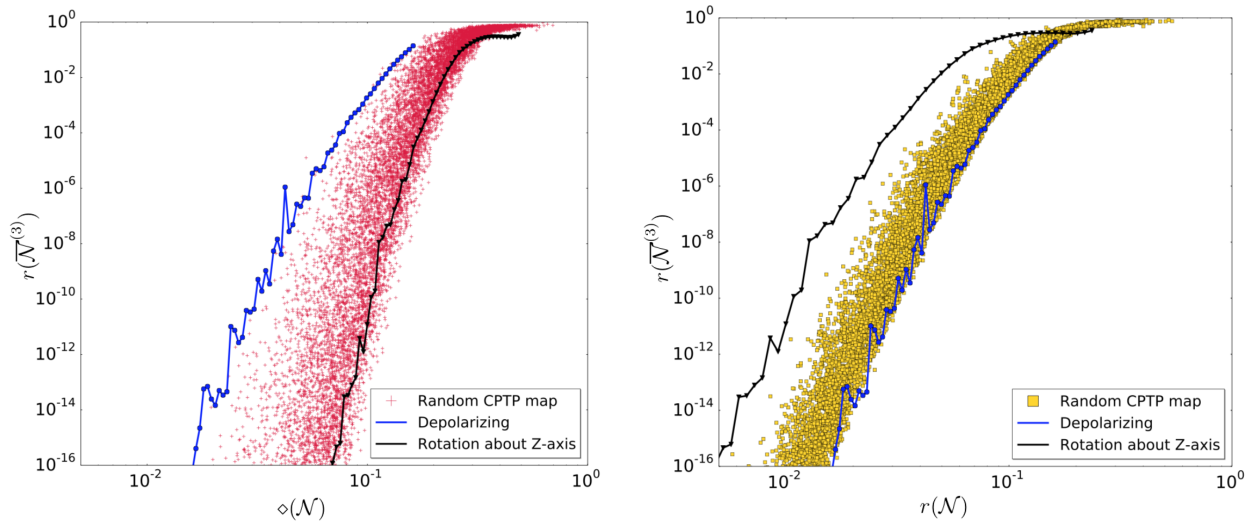

Figure 1.9: Plots of average logical fidelity for an encoded noisy state at the third level of concatenation, $r(\overline{\mathcal{N}}^{(3)})$, in the Steane code entangled with a perfect single qubit state as a function of physical diamond distance, $\diamond(\mathcal{N})$, (left) and physical infidelity, $r(\mathcal{N})$, (right) when recovery operations are selected to maximize fidelity with the noiseless state [23]. Each point on each plot corresponds to a random CPTP map, which acts on each physical qubit comprising the state encoded in the Steane code. The blue lines show the behaviour of depolarizing noise, while the black show the scaling of errors for a coherent rotation about the Z axis.

1.7.1 Current Experimental Error Rates

Several companies have developed quantum computing devices. This section presents the error rates and number of qubits for some of these devices, as well as plans for future devices to demonstrate scalability. Error rates are presented in terms of infidelity for single-qubit (two-qubit) gates averaged over each qubit, r_{1q} (r_{2q}), and readout error, e_{RO}, corresponding to the error introduced by preparing and immediately measuring a state. Rigetti defines the readout error as $e_{RO} = \frac{1}{2}[p(0|0) + p(1|1)]$, where $p(x|y)$ is the probability of measuring x given that the state prepared was y [24].

Company/Acedemic Group	Name of Device	Number of Qubits	r_{1q}	r_{2q}	e_{RO}
Blatt [25]	NR	20	NR	NR	NR
IBM [26]	IBM Q 20 Austin	20	0.010	[17]0.0638	0.1479
IBM [26]	IBM Q 20 Tokyo	20	0.002	0.0287	0.077
Intel [27]	NR	17	NR	NR	NR
Intel [28]	Tangle Lake	49	NR	NR	NR
Google [29]	NR	9	[18]0.0008	NR	0.022
Monroe [30]	NR	5	[19]NR	0.017	NR
Rigetti [24]	NR	20	0.0137	0.123	0.067

Table 1.5: Number of qubits and error rates in current quantum devices, as reported by the companies developing each device. NR indicates that the value was not reported in the cited articles, or that no value listed is clearly associated with these error metrics.

Google has announced plans to build Bristlecone, a 72-qubit quantum device, using devices modeled after their 9-qubit device as unit blocks with the goal of achieving error rates as low as those in the 9-qubit device [31]. Rigetti unveiled plans to build a 152-qubit quantum device by August 2019 using blocks of 16-qubits [32].

To achieve quantum supremacy, ie for a quantum computer to outperform current state of the art classical computers, Google believes (As of March, 2018) that a quantum computer would require 49 qubits, a two-qubit gate infidelity of less than 0.5%, and to be able to perform circuits with a circuit depth of 40 [31]. Current devices with fewer than 49 qubits have been shown to exceed a 2-qubit gate infidelity of 0.5% by an order of magnitude (see table 1.5), though circuits with more than 40 gates have been achieved on these smaller devices [24]. Devices which meet the aforementioned size criteria are presently being developed or have been announced, though error rates have not yet been published for these larger devices, and there is as of yet no evidence that they have met the circuit length requirement.

[17] IBM reports this as a multi-qubit gate error for both of their 20-qubit devices.

[18] Note that the average single-qubit gate fidelity was only measured for 4 of the 9 qubits, and this is an average over those 4 qubits.

[19] The Monroe group reports an average infidelity of 0.02 for a set of single- and 2-qubit gates.

1.8 The Process Matrix Formalism

Process matrices are another way to express channels. The size of a process matrix for a single logical state is fixed by the chosen basis so that the dimensions do not increase with increasing code distance; this allows for a significant reduction in computational complexity in the simulation of quantum channels. Further, successive operations are captured in the process matrix formalism by a simple matrix multiplication rather than by nesting sums of conjugations, as in the Kraus formalism, allowing for simulation of significantly more complicated channels. The use of process matrices for quantum channels was originally suggested by Rahn *et. al* in 2002 [33], and they have since been used to calculate thresholds[20] at high levels of concatenation [10], and examine the contribution of coherent errors at the logical level [34]. This section introduces the process matrix formalism and shows the derivation for process matrices at various stages of the error correcting process. The expressions for single-qubit noise and noise after full error correction were shown in [33], while the expressions for encoded noise with no error correction and encoded noise after syndrome measurement are new.

The set of Pauli matrices, $\mathbb{P} = \{I, X, Y, Z\}$, forms a basis for Hermitian matrices in $\mathbb{C}^{2\times 2}$, so that we can write an arbitrary quantum state as

$$\rho = \frac{1}{\sqrt{2}}[\langle I\rangle_\rho I + \langle X\rangle_\rho X + \langle Y\rangle_\rho Y + \langle Z\rangle_\rho Z], \tag{1.28}$$

where $\langle\sigma\rangle_\tau$ is the expectation value of σ for the state τ. Then let

$$|\rho\rangle\!\rangle = \frac{1}{\sqrt{2}}\begin{bmatrix}\langle I\rangle_\rho \\ \langle X\rangle_\rho \\ \langle Y\rangle_\rho \\ \langle Z\rangle_\rho\end{bmatrix}, \tag{1.29}$$

to arrive at a representation of an q-dimensional quantum state in the process matrix formalism. More generally, a state ρ can be written in terms of an arbitrary trace-orthonormal basis of $\mathbb{C}^{q\times q}$, $\{B_i\}$, as

$$\rho = \sum_i \mathrm{Tr}(B_i^\dagger \rho) B_i. \tag{1.30}$$

[20] Bounds on the physical noise parameters for which a QECC can correct errors

Vectorizing by letting $|B_i\rangle\rangle \to e_i$, where $\{e_i\}$ is the canonical basis of $\mathbb{C}^{q^2}$, we arrive at the representation of a state in the process matrix formalism,

$$|\rho\rangle\rangle = \sum_i \mathrm{Tr}[B_i^\dagger \rho] e_i. \tag{1.31}$$

In the Pauli basis, a channel, $\mathcal{V} : \rho_i \to \rho_f$, is expressed as a 4×4 matrix such that $|\rho_f\rangle\rangle = \mathcal{V}|\rho_i\rangle\rangle$.

From eq. (1.31), and letting $\langle\langle\rho| = |\rho\rangle\rangle^\dagger$, we derive below an expression for $\langle\langle\rho|\tau\rangle\rangle$,

$$\langle\langle\rho|\tau\rangle\rangle = \sum_{i,j} \mathrm{Tr}(\rho^\dagger B_i) e_i^\dagger \mathrm{Tr}(B_j^\dagger \tau) e_j \tag{1.32}$$

$$= \sum_i \mathrm{Tr}(\rho^\dagger B_i)\mathrm{Tr}(B_i^\dagger \tau). \tag{1.33}$$

Recalling the decomposition of matrices given in eq. (1.30),

$$\mathrm{Tr}(\rho^\dagger \tau) = \sum_{i,j} \mathrm{Tr}(B_i^\dagger \rho)^* \mathrm{Tr}(B_j \tau)\mathrm{Tr}(B_i^\dagger B_j) \tag{1.34}$$

$$= \sum_i \mathrm{Tr}(\rho^\dagger B_i)\mathrm{Tr}(B_i \tau). \tag{1.35}$$

So that

$$\langle\langle\rho|\tau\rangle\rangle = \mathrm{Tr}(\rho^\dagger \tau). \tag{1.36}$$

1.8.1 Noise in A Quantum Channel

The process of quantum error correction on a noisy communication or memory channel can be described by a channel, $\overline{\mathcal{N}}(R_m)$, which encodes a logical state via a map $\mathcal{C}$, exposes it to some noise, $\mathcal{N}$, measures a syndrome, m, and applies recovery operation R_m, both captured by $\mathcal{R}$, and then decodes, with $\mathcal{D}$, is given by

$$\overline{\mathcal{N}}(R_m) = \mathcal{D}\mathcal{R}\mathcal{N}\mathcal{C}, \tag{1.37}$$

where the bar over $\mathcal{N}$ in $\overline{\mathcal{N}}(R_m)$ is used to denote logical noise. This entire process is shown in fig. 1.10.

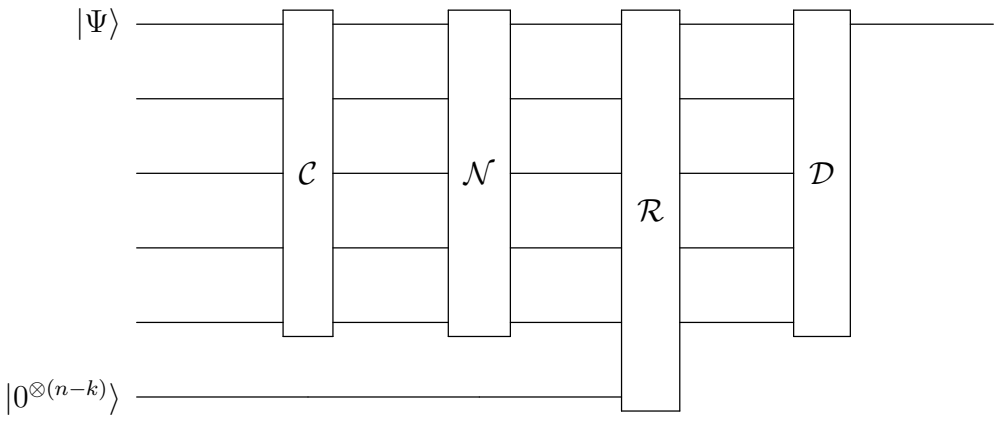

Figure 1.10: Quantum circuit diagram depicting the encoding of a state, Ψ, in a quantum error correcting code. The encoded state then undergoes some noise, $\mathcal{N}$, and a syndrome measurement and recovery operation are applied by $\mathcal{R}$ before the state is decoded by $\mathcal{D}$.

The matrix $\overline{\mathcal{N}}(R_m)$ can be thought of as a noisy communications channel or quantum memory. Alternatively, we can model an encoded computation by replacing $\mathcal{N}$ with a series of encoded gates. In this work, we study the effects of quantum error correction on physical noise processes. As such, we will restrict attention to the channel $\overline{\mathcal{N}}(R_m)$ described above, and assume perfect $\mathcal{C}$, $\mathcal{R}$, and $\mathcal{D}$.

1.8.2 Infidelity as a Function of the Process Matrix

Here we derive an expression for the infidelity of a channel, $\mathcal{N}$, in terms of its process matrix representation. Recalling the expression for infidelity in terms of the channel's Kraus operators, $\{A_k\}$, from eq. (1.24),

$$r(\mathcal{N}) = \frac{\sum_k |\mathrm{Tr}(A_k)|^2 + q}{q(q+2)}, \tag{1.38}$$

we note that in order to express the infidelity in terms of the process matrix of the channel rather than its Kraus operators, we must simply re-write $\sum_k |\mathrm{Tr}(A_k)|^2$. We define $\{B_\sigma\}$ as the orthonormal Pauli basis, $\mathbb{P}/\sqrt{2}$. Starting from the trace of the process matrix,

$$\mathrm{Tr}(\mathcal{N}) = \mathrm{Tr}\left(\sum_{\sigma,k} B_\sigma A_k B_\sigma A_k^\dagger\right) \tag{1.39}$$

$$= \sum_{\sigma,k} \mathrm{Tr}(B_\sigma A_k B_\sigma A_k^\dagger). \tag{1.40}$$

From eq. (1.35),

$$\sum_{\sigma,k} \mathrm{Tr}(B_\sigma A_k B_\sigma A_k^\dagger) = \sum_{i,\sigma,k} \mathrm{Tr}(B_\sigma A_k^\dagger B_i)\mathrm{Tr}(B_i B_\sigma A_k). \tag{1.41}$$

Because $B_\sigma = B_\sigma^\dagger$ and $\{B_\sigma\}$ is an orthonormal basis,

$$\mathrm{Tr}(B_\sigma A_k B_\sigma^\dagger A_k^\dagger) = \sum_k \mathrm{Tr}(A_k^\dagger)\mathrm{Tr}(A_k) \tag{1.42}$$

$$= \sum_k |\mathrm{Tr}(A_k)|^2, \tag{1.43}$$

So from eq. (1.40),

$$\mathrm{Tr}(\mathcal{N}) = \sum_k |\mathrm{Tr}(A_k)|^2. \tag{1.44}$$

The infidelity in terms of the process matrix of the channel is then

$$r(\mathcal{N}) = \frac{\mathrm{Tr}(\mathcal{N}) + q}{q(q+1)}, \tag{1.45}$$

where $\mathcal{N}$ is acting on a q-dimensional state. For a qubit,

$$r(\mathcal{N}) = \frac{\mathrm{Tr}(\mathcal{I} - \mathcal{N})}{6} \tag{1.46}$$

1.8.3 Quantum Channels in the Process Matrix Formalism

Noise on an Unencoded State

The final state after undergoing some channel, $\mathcal{N} : \rho_i \to \rho_f$, is described by

$$\langle B_i \rangle_{\rho_f} = \mathrm{Tr}[B_i \rho_f] \tag{1.47}$$
$$= \mathrm{Tr}[B_i \mathcal{N}[\rho_i]] \tag{1.48}$$
$$= \mathrm{Tr}\left[B_i \mathcal{N}\left[\sum_j \langle B_j \rangle_{\rho_i} B_j \right] \right] \tag{1.49}$$
$$\tag{1.50}$$

Expanding $|\rho_f\rangle\rangle = \mathcal{N}|\rho_i\rangle\rangle$, we arrive at the following expression for the elements of $\mathcal{N}$

$$\mathcal{N}_{B_i,B_j} = \mathrm{Tr}[B_i \mathcal{N}[B_j]]. \tag{1.51}$$

In the Pauli basis,

$$\mathcal{N}_{\sigma,\sigma'} = \frac{1}{2}\mathrm{Tr}[\sigma \mathcal{N}[\sigma']], \tag{1.52}$$

where $\sigma, \sigma' \in \mathbb{P}$, and the $1/2$ comes from normalization. We continue in the Pauli basis for the remainder of this thesis.

Noise on an Encoded State

This section derives an expression for the effective logical noise arising from physical noise $\mathcal{N}$ when no syndrome measurement or recovery operations are applied.

In the Kraus operator formalism, an encoding channel can be expressed as

$$\mathcal{C}[\rho] = C\rho C^\dagger, \tag{1.53}$$

where $C = |\overline{0}\rangle\langle 0| + |\overline{1}\rangle\langle 1|$ for a single logical qubit, and

$$C = \sum_{b \in \mathbb{Z}_2^k} |\overline{b}\rangle\langle b| \tag{1.54}$$

for a k-qubit encoding. The corresponding decoding is then given by $\mathcal{D}[\mathcal{C}[\rho]] = C^\dagger \mathcal{C}[\rho] C$ for an arbitrary encoded state, $\mathcal{C}[\rho]$. Encoding $\mathbb{P}$ gives $\mathbb{E} = \{E_\sigma\}$, $\sigma \in \mathbb{P}$. An encoded state can be expressed as

$$\mathcal{C}[\rho] = \frac{1}{2^k} \sum_\sigma \mathrm{Tr}[\langle \sigma \rangle_\rho E_\sigma]. \tag{1.55}$$

For a single logical qubit,

$$\mathcal{C}[\rho] = \frac{1}{2^k} \mathrm{Tr}[\langle I \rangle_\rho E_I + \langle X \rangle_\rho E_X + \langle Y \rangle_\rho E_Y + \langle Z \rangle_\rho E_Z], \tag{1.56}$$

where

$$E_I = |\overline{0}\rangle\langle\overline{0}| + |\overline{1}\rangle\langle\overline{1}| \tag{1.57}$$
$$E_Z = |\overline{0}\rangle\langle\overline{0}| - |\overline{1}\rangle\langle\overline{1}| \tag{1.58}$$
$$E_X = |\overline{0}\rangle\langle\overline{1}| + |\overline{1}\rangle\langle\overline{0}| \tag{1.59}$$
$$E_Y = i(|\overline{0}\rangle\langle\overline{1}| - |\overline{1}\rangle\langle\overline{0}|). \tag{1.60}$$

The final state, after encoding, $\mathcal{C}$, undergoing some noise process, $\mathcal{N}$, and decoding, $\mathcal{D}$, is described by

$$\langle \sigma \rangle_{\rho_f} = \mathrm{Tr}[\sigma \rho_f] \tag{1.61}$$
$$= \mathrm{Tr}[\sigma C^\dagger \mathcal{N}[\mathcal{C}[\rho_i]] C] \tag{1.62}$$
$$= \mathrm{Tr}[E_\sigma \mathcal{N}[\mathcal{C}[\rho_i]]]. \tag{1.63}$$

The action of $\mathcal{N}$ on the encoded state will map some terms in the expansion of the state out of the codespace; these terms will be lost when the decoding map is applied, so that the effective channel is trace decreasing when neither syndrome measurements nor recovery operations are applied. The effective channel is given by

$$\overline{\mathcal{N}}_{\sigma,\sigma'} = \frac{1}{2^k} \mathrm{Tr}[E_\sigma \mathcal{N}[E_{\sigma'}]], \tag{1.64}$$

where the factor of $1/2^k$ arises to normalize the $\{E_\sigma\}$ so that they form an orthonormal basis. The encoded Pauli operator, E_σ, acts on the codespace as $\overline{\sigma}$ and vanishes elsewhere. We define an operator, Π_0, which projects onto the codespace[21],

$$\Pi_{m_0} = \frac{1}{|\mathbb{S}|} \sum_{S \in \mathbb{S}} S, \tag{1.65}$$

and construct an operator which projects onto the codespace and acts as $\overline{\sigma}$, so that we can write

$$E_\sigma = \Pi_{m_0} \overline{\sigma} \tag{1.66}$$

$$= \frac{1}{|\mathbb{S}|} \sum_{S \in \mathbb{S}} S\overline{\sigma}. \tag{1.67}$$

Substituting eq. (1.67) into eq. (1.64), we arrive at eq. (1.68),

$$\overline{\mathcal{N}}_{\sigma,\sigma'} = \frac{1}{2^k |\mathbb{S}|^2} \sum_{S,S' \in \mathbb{S}} \mathrm{Tr}[S\overline{\sigma}\mathcal{N}[S'\overline{\sigma}']]. \tag{1.68}$$

By eq. (1.36),

$$\overline{\mathcal{N}}_{\sigma,\sigma'} = \frac{1}{2^k |\mathbb{S}|^2} \sum_{S,S' \in \mathbb{S}} \langle\langle S\overline{\sigma}|\mathcal{N}|S'\overline{\sigma}'\rangle\rangle. \tag{1.69}$$

Expanding $\langle\langle S\overline{\sigma}|\mathcal{N}|S'\overline{\sigma}'\rangle\rangle$[22],

$$\langle\langle S\overline{\sigma}|\mathcal{N}|S'\overline{\sigma}'\rangle\rangle = 2^n \chi(S\overline{\sigma})\chi(S'\overline{\sigma}') \prod_{j \in \mathbb{Z}_n} \mathcal{N}^{(j)}_{(S\overline{\sigma})_j,(S'\overline{\sigma}')_j}, \tag{1.70}$$

where $\chi(A)$ is the global phase of A relative to a member of $\mathbb{P}_n$ such that $\exists B \in \mathbb{P}_n$ with $\chi(A)B = A$. Thus,

$$\overline{\mathcal{N}}_{\sigma,\sigma'} = \frac{1}{|\mathbb{S}|} \sum_{S,S' \in \mathbb{S}} \chi(S\overline{\sigma})\chi(S'\overline{\sigma}') \prod_{j \in \mathbb{Z}_n} \mathcal{N}^{(j)}_{(S\overline{\sigma})_j,(S'\overline{\sigma}')_j}. \tag{1.71}$$

[21] Recall that we previously defined $\mathbb{S}$ as the stabilizer group of a quantum error correcting code.

[22] The full derivation of this equation is given in appendix A

Effective Noise after Syndrome Measurement

In an error correcting protocol, after exposure to some noise, $\mathcal{N}$, the encoded state is projected onto a cospace associated with syndrome m by a projection operator, Π_m, with some probability, $p(m)$. The projection operator corresponding to syndrome m is given by eq. (1.22). The resultant state is described by $\{\langle\sigma\rangle_f\}$, where

$$\begin{aligned}\langle\sigma\rangle_{\rho_f} &= \mathrm{Tr}[\sigma\rho_f] && (1.72)\\ &= \frac{1}{p(m)}\mathrm{Tr}[\sigma C^\dagger \Pi_m \mathcal{N}[\mathcal{C}[\rho_i]]\Pi_m^\dagger C] && (1.73)\\ &= \frac{1}{p(m)}\mathrm{Tr}[\Pi_m^\dagger C\sigma C^\dagger \Pi_m \mathcal{N}[\mathcal{C}[\rho_i]]] && (1.74)\\ &= \frac{1}{p(m)}\mathrm{Tr}[\Pi_m^\dagger E_\sigma \Pi_m \mathcal{N}[\mathcal{C}[\rho_i]]]. && (1.75)\end{aligned}$$

Let $\mathcal{P}_m[\rho] = \frac{1}{p(m)}\Pi_m\rho\Pi_m$ so that

$$\langle\sigma\rangle_{\rho_f} = \mathrm{Tr}\left[\mathcal{P}_m[E_\sigma]\mathcal{N}\left[\frac{1}{2^k}\sum_{\sigma'}\langle\sigma'\rangle_{\rho_i}E_{\sigma'}\right]\right]. \tag{1.76}$$

By eq. (1.36),

$$\langle\sigma\rangle_{\rho_f} = \langle\!\langle E_\sigma|\mathcal{P}_m^\dagger\mathcal{N}|\frac{1}{2^k}\sum_{\sigma'}\langle\sigma'\rangle_{\rho_i}E_{\sigma'}\rangle\!\rangle. \tag{1.77}$$

Expanding $|\rho_f\rangle\!\rangle = \mathcal{E}|\rho_i\rangle\!\rangle$ for an arbitrary channel, $\mathcal{E}$, it is clear that

$$\begin{aligned}\overline{\mathcal{N}}_{\sigma,\sigma'}(m) &= \frac{1}{2^k}\langle\!\langle E_\sigma|\mathcal{P}_m^\dagger\mathcal{N}|E_{\sigma'}\rangle\!\rangle && (1.78)\\ &= \frac{1}{2^k p(m)}\langle\!\langle \Pi_m E_\sigma \Pi_m|\mathcal{N}|E_{\sigma'}\rangle\!\rangle. && (1.79)\end{aligned}$$

Substituting eq. (1.67) into eq. (1.79),

$$\overline{\mathcal{N}}_{\sigma,\sigma'}(m) = \frac{1}{2^k p(m)|\mathbb{S}|^2}\sum_{S,S'\in\mathbb{S}}\langle\!\langle \Pi_m S\overline{\sigma}\Pi_m|\mathcal{N}|S'\overline{\sigma}'\rangle\!\rangle. \tag{1.80}$$

Because logical operators commute with stabilizers, and Π_m can be written as an sum of stabiliers,

$$\overline{\mathcal{N}}_{\sigma,\sigma'}(m) = \frac{1}{2^k p(m)|\mathbb{S}|^2} \sum_{S,S'\in\mathbb{S}} \langle\langle \Pi_m S \Pi_m \overline{\sigma}|\mathcal{N}|S'\overline{\sigma}'\rangle\rangle. \tag{1.81}$$

Projecting a sum over stabilizer elements onto a codespace introduces signs such that

$$\sum_{S\in\mathbb{S}} \Pi_m S \Pi_m = \Pi_m. \tag{1.82}$$

Then,

$$\overline{\mathcal{N}}_{\sigma,\sigma'}(m) = \frac{1}{2^k p(m)|\mathbb{S}|^2} \sum_{S,S'\in\mathbb{S}} \nu(S|m)\langle\langle S\overline{\sigma}|\mathcal{N}|S'\overline{\sigma}'\rangle\rangle, \tag{1.83}$$

where $\nu(S|m)$ is the sign of S in the expansion of Π_m in eq. (1.22). Using eq. (1.70),

$$\overline{\mathcal{N}}_{\sigma,\sigma'}(m) = \frac{2^n}{2^k p(m)|\mathbb{S}|^2} \sum_{S,S'\in\mathbb{S}} \nu(S|m)\chi(S\overline{\sigma})\chi(S'\overline{\sigma}') \prod_{j\in\mathbb{Z}_n} \mathcal{N}^{(j)}_{(S\overline{\sigma})_j,(S'\overline{\sigma}')_j} \tag{1.84}$$

$$= \frac{1}{p(m)|\mathbb{S}|} \sum_{S,S'\in\mathbb{S}} \nu(S|m)\chi(S\overline{\sigma})\chi(S'\overline{\sigma}') \prod_{j\in\mathbb{Z}_n} \mathcal{N}^{(j)}_{(S\overline{\sigma})_j,(S'\overline{\sigma}')_j}. \tag{1.85}$$

It is often convenient to sum over recovery operations to get a picture of how the channel acts on average. This is described by

$$\langle\overline{\mathcal{N}}_{\sigma,\sigma'}\rangle_{(\backslash R)} = \frac{1}{|\mathbb{S}|} \sum_{\substack{m\in\mathbb{Z}_2^{n-k} \\ S,S'\in\mathbb{S}}} \nu(S|m)\chi(S\overline{\sigma})\chi(S'\overline{\sigma}') \prod_{j\in\mathbb{Z}_n} \mathcal{N}^{(j)}_{(S\overline{\sigma})_j,(S'\overline{\sigma}')_j}. \tag{1.86}$$

Effective Noise with Full Error Correction

In an error correcting protocol, after a state has been exposed to some noise, a projective measurement, Π_m, projects the resultant state onto a cospace associated with syndrome

$m \in \mathbb{Z}_2^{n-k}$ with some probability, $p(m)$. A recovery operation, $R_m \in \mathbb{R}$, is then applied to map the state back to the codespace. This mapping acts on a state, ρ, as

$$\overline{\mathcal{N}}(\rho, R_m) = \mathcal{R}_m[\mathcal{N}[\mathcal{C}[\rho]]] = \frac{1}{p(m)} R_m \Pi_m \mathcal{N}[\mathcal{C}[\rho]] \Pi_m^\dagger R_m^\dagger, \tag{1.87}$$

where $\mathcal{R}_m$ projects onto the cospace corresponding to syndrome m and applies R_m.

As described in section 1.8.3: *Effective Noise after Syndrome Measurement*, it is often convenient to sum over syndrome measurements to analyse the channel in its entirety; we refer to the resultant process matrix as the average channel. We therefore do the same here. Letting $\langle\overline{\mathcal{N}}(\rho)\rangle$ be the effective logical channel averaged over recovery operations,

$$\langle\overline{\mathcal{N}}(\rho)\rangle = \mathcal{R}[\mathcal{N}[\mathcal{C}[\rho]]] = \sum_m \frac{1}{p(m)} R_m \Pi_m \mathcal{N}[\mathcal{C}[\rho]] \Pi_m^\dagger R_m^\dagger. \tag{1.88}$$

The average final state, ρ_f, after encoding, exposing the encoded state to some noise, $\mathcal{N}$, measuring syndromes, applying recovery operations, and decoding will be specified by the expectation values of the Pauli operators, $\{\langle\sigma\rangle_{\rho_f}\}$,

$$\begin{aligned}
\langle\sigma\rangle_{\rho_f} &= \mathrm{Tr}[\sigma\rho_f] && (1.89)\\
&= \mathrm{Tr}\left[\sum_m \sigma C^\dagger R_m \Pi_m \mathcal{N}[\mathcal{C}[\rho_i]] \Pi_m^\dagger R_m^\dagger C\right] && (1.90)\\
&= \mathrm{Tr}\left[\sum_m \Pi_m^\dagger R_m^\dagger C \sigma C^\dagger R_m \Pi_m \mathcal{N}[\mathcal{C}[\rho_i]]\right] && (1.91)\\
&= \mathrm{Tr}\left[\sum_m \Pi_m^\dagger R_m^\dagger E_\sigma R_m \Pi_m \mathcal{N}[\mathcal{C}[\rho_i]]\right] && (1.92)\\
&= \mathrm{Tr}[D_\sigma \mathcal{N}[\mathcal{C}[\rho_i]]], && (1.93)
\end{aligned}$$

where $D_\sigma = \sum_m \Pi_m^\dagger R_m^\dagger E_\sigma R_m \Pi_m$. Then,

$$\langle\sigma\rangle_{\rho_f} = \mathrm{Tr}\left[D_\sigma \mathcal{N}\left[\frac{1}{2^k}\sum_{\sigma'}\langle\sigma'\rangle_{\rho_i} E_{\sigma'}\right]\right]. \tag{1.94}$$

Expanding $|\rho_f\rangle\!\rangle = \overline{\mathcal{N}}|\rho_i\rangle\!\rangle$, we arrive at an expression for the elements of $\langle\overline{\mathcal{N}}\rangle$, the average effective logical process matrix after full error correction has been applied,

$$\langle\overline{\mathcal{N}}_{\sigma,\sigma'}\rangle = \frac{1}{2^k}\mathrm{Tr}[D_\sigma \mathcal{N}[E_{\sigma'}]]. \tag{1.95}$$

Then, using eq. (1.67),

$$D_\sigma = \frac{1}{|\mathbb{S}|}\sum_{\substack{m\in\mathbb{Z}_2^{n-k}\\ S\in\mathbb{S}}} \Pi_m^\dagger R_m^\dagger S\overline{\sigma} R_m \Pi_m \tag{1.96}$$

Because the stabilizers, logical operators, and recovery operators are all Pauli, they will either commute or anti-commute. So we define $\eta(A,B)$ implicitly as $AB = \eta(A,B)BA$ and commute R_m past $S\overline{\sigma}$. Because $R_m^\dagger R_m = 1$, and recalling eq. (1.82),

$$D_\sigma = \frac{1}{|\mathbb{S}|}\sum_{\substack{R\in\mathbb{R}\\ S\in\mathbb{S}}} \eta(S\overline{\sigma}, R) S\overline{\sigma}, \tag{1.97}$$

where $\eta(A,B)AB = BA$. Substituting eq. (1.67) and eq. (1.97) into eq. (1.95),

$$\langle\overline{\mathcal{N}}_{\sigma,\sigma'}\rangle = \frac{1}{2^k|\mathbb{S}|^2}\sum_{\substack{S,S'\in\mathbb{S}\\ R\in\mathbb{R}}} \eta(S\overline{\sigma}, R)\mathrm{Tr}[S\overline{\sigma}\mathcal{N}[S'\overline{\sigma}']]. \tag{1.98}$$

By eq. (1.36),

$$\langle\overline{\mathcal{N}}_{\sigma,\sigma'}\rangle = \frac{1}{2^k|\mathbb{S}|^2}\sum_{\substack{S,S'\in\mathbb{S}\\ R\in\mathbb{R}}} \eta(S\overline{\sigma}, R)\langle\!\langle S\overline{\sigma}|\mathcal{N}|S'\overline{\sigma}'\rangle\!\rangle. \tag{1.99}$$

From eq. (1.70),

$$\langle\overline{\mathcal{N}}_{\sigma,\sigma'}\rangle = \frac{1}{|\mathbb{S}|}\sum_{\substack{S,S'\in\mathbb{S}\\ R\in\mathbb{R}}} \eta(S\overline{\sigma}, R)\chi(S\overline{\sigma})\chi(S'\overline{\sigma}')\prod_{j\in\mathbb{Z}_n}\mathcal{N}^{(j)}_{(S\overline{\sigma})_j,(S'\overline{\sigma}')_j}. \tag{1.100}$$

1.8.4 Examples of Operations in the Process Matrix Formalism

This section presents some basic operations in the process matrix formalism. The Pauli operators are

$$\mathcal{X} = \begin{bmatrix} 1 & 0 & 0 & 0 \\ 0 & 1 & 0 & 0 \\ 0 & 0 & -1 & 0 \\ 0 & 0 & 0 & -1 \end{bmatrix} \quad \mathcal{Y} = \begin{bmatrix} 1 & 0 & 0 & 0 \\ 0 & -1 & 0 & 0 \\ 0 & 0 & 1 & 0 \\ 0 & 0 & 0 & -1 \end{bmatrix} \quad \mathcal{Z} = \begin{bmatrix} 1 & 0 & 0 & 0 \\ 0 & -1 & 0 & 0 \\ 0 & 0 & -1 & 0 \\ 0 & 0 & 0 & 1 \end{bmatrix}. \tag{1.101}$$

Recalling the unitary rotation channel defined in section 1.2.1, a rotation about the x-axis by θ is given by

$$\mathcal{R}_x(\theta) = \begin{bmatrix} 1 & 0 & 0 & 0 \\ 0 & 1 & 0 & 0 \\ 0 & 0 & \cos 2\theta & \sin 2\theta \\ 0 & 0 & -\sin 2\theta & \cos 2\theta \end{bmatrix}. \tag{1.102}$$

Analogously, process matrices for rotations about the y-axis, z-axis, and the axis equidistant from the x, y, and z axes, defined by $\vec{n} = (1/\sqrt{3}, 1/\sqrt{3}, 1/\sqrt{3})$ are

$$\mathcal{R}_y(\theta) = \begin{bmatrix} 1 & 0 & 0 & 0 \\ 0 & \cos 2\theta & 0 & -\sin 2\theta \\ 0 & 0 & 1 & 0 \\ 0 & \sin 2\theta & 0 & \cos 2\theta \end{bmatrix}, \quad \mathcal{R}_z(\theta) = \begin{bmatrix} 1 & 0 & 0 & 0 \\ 0 & \cos 2\theta & \sin 2\theta & 0 \\ 0 & -\sin 2\theta & \cos 2\theta & 0 \\ 0 & 0 & 0 & 1 \end{bmatrix}, \tag{1.103}$$

and

$$\mathcal{R}_{xyz} = \begin{bmatrix} 1 & 0 & 0 & 0 \\ 0 & \frac{1}{3}(1+2\cos 2\theta) & \frac{2}{3}\sin\theta(\sin\theta+\sqrt{3}\cos\theta) & \frac{2}{3}\sin\theta(\sin\theta-\sqrt{3}\cos\theta) \\ 0 & \frac{2}{3}\sin\theta(\sin\theta-\sqrt{3}\cos\theta) & \frac{1}{3}(1+2\cos 2\theta) & \frac{2}{3}\sin\theta(\sin\theta+\sqrt{3}\cos\theta) \\ 0 & \frac{2}{3}\sin\theta(\sin\theta+\sqrt{3}\cos\theta) & \frac{2}{3}\sin\theta(\sin\theta-\sqrt{3}\cos\theta) & \frac{1}{3}(1+2\cos 2\theta) \end{bmatrix}, \tag{1.104}$$

respectively. The depolarizing channel defined in section 1.2.1 is

$$\mathcal{D}_p = \begin{bmatrix} 1 & 0 & 0 & 0 \\ 0 & 1-p & 0 & 0 \\ 0 & 0 & 1-p & 0 \\ 0 & 0 & 0 & 1-p \end{bmatrix}. \tag{1.105}$$

Chapter 2

Quantum Error Correction: When Errors Happen, what is the Impact?

In this chapter, we explore the effects of quantum error correction on physical noise processes. We first discuss the form of noise from a quantum channel at the physical level, before extending our discussion to the effective logical noise post-syndrome measurement and after the application of recovery operations. We demonstrate that syndrome measurement suppresses the non-Pauli components of the noise, and show that the selection of recovery operations effectively dictates the severity of the average effective logical noise. Further, we discuss the usefulness of the logical fidelity as a measure of the efficacy of a set of recovery operations. Many of the results presented in section 2.1-2.3 of this chapter were released in [35] prior to the completion of this document.

2.1 Bounds on Noise Processes

Let $\mathcal{E} = |\mathcal{I} - \mathcal{N}|$ be the error process matrix.

Lemma 14. *For any single-qubit Markovian noise channel with infidelity, $r \leq 1/3$,*

$$\mathcal{E}_{I,\sigma'} = 0 \tag{2.1a}$$

$$\mathcal{E}_{\sigma,I} \leq 3r \tag{2.1b}$$

$$\mathcal{E}_{\sigma,\sigma} \leq 3r \tag{2.1c}$$

$$\mathcal{E}_{\sigma,\sigma'} \leq \sqrt{6r - 9r^2} \tag{2.1d}$$

where $\sigma, \sigma' \in (\mathbb{P}\backslash I)/\sqrt{2}$.

Proof. Equation (2.1a) follows directly from the trace-preserving condition on quantum channels; recall that $\mathcal{N}_{\sigma,\sigma'} = \frac{1}{2}\mathrm{Tr}(\sigma\mathcal{N}[\sigma']))$ from eq. (1.52), and $\mathrm{Tr}(\sigma') = 2\delta_{I,\sigma'} \forall \sigma' \in \mathbb{P}$. For any CPTP map, $\mathcal{N}$, then, $\mathrm{Tr}(\mathcal{N}[\sigma']) = 2\delta_{I,\sigma'} \forall \sigma' \in \mathbb{P}$, and $\mathcal{N}_{I,\sigma'} = \mathrm{Tr}(I\mathcal{N}[\sigma']) = 2\delta_{I,\sigma'} \forall \sigma' \in \mathbb{P}$.

Equation (2.1b) was shown in [19, Prop. 12].

The proof of eq. (2.1c) is an extension of the proof of [19, Prop 12], where we note that taking the Pauli twirl of $\mathcal{N}$ produces a diagonal matrix with the singular values of $\mathcal{N}$ on the diagonal. Analogous to the proof of [19, Prop 12], we write $\mathcal{N}_{\sigma,\sigma} = 1 - \gamma_\sigma r$, for $\gamma_\sigma \geq 0$, so that $\mathcal{E}_{\sigma,\sigma} = \gamma_\sigma r$, where the $\{\gamma_\sigma\}$ must satisfy

$$(\gamma_\sigma - \gamma_\tau)^2 \leq \gamma_\zeta^2 \tag{2.2}$$

for all permutations $\{\sigma, \tau, \zeta\}$ of $\mathbb{P}\backslash I$ by [19, eq. 63]. Rearranging eq. (1.46),

$$\sum_{\sigma \in \mathbb{P}\backslash I} \mathcal{N}_{\sigma,\sigma} = 3 - 6r \tag{2.3}$$

$$= 3 - (\gamma_\sigma + \gamma_\tau + \gamma_\zeta)r, \tag{2.4}$$

it is clear that $\sum_\sigma \gamma_\sigma = 6$. Combined with eq. (2.2), we can conclude that $\gamma_\sigma \leq 3 \forall \sigma \in \mathbb{P}\backslash I$.

To prove eq. (2.1d), we first define the unital part, $\mathcal{M}_u$, of a process matrix, $\mathcal{M}$, as the sub-matrix obtained by deleting the first row and column of $\mathcal{M}$.

King and Ruskai, [36], [37], showed that a process matrix for a valid channel can be written as

$$\mathcal{M} \approx \begin{bmatrix} 1 & 0 & 0 & 0 \\ t_1 & \lambda_1 & 0 & 0 \\ t_2 & 0 & \lambda_2 & 0 \\ t_3 & 0 & 0 & \lambda_3 \end{bmatrix}, \tag{2.5}$$

up to a change of basis, where the $|\lambda_i|$ are the singular values of $\mathcal{M}_u$. Applying this approximation of $\mathcal{M}$ x times will cause the λ_i to go to their x^{th} power. If any λ_i is ≥ 1 then that singular value will diverge. Thus, the λ_i are upper-bounded by 1. Including the change of basis, we can write [19]

$$\mathcal{M} = (I \oplus U) \begin{bmatrix} 1 & 0 & 0 & 0 \\ 0 & \lambda_1 & 0 & 0 \\ 0 & 0 & \lambda_2 & 0 \\ t & 0 & 0 & \lambda_3 \end{bmatrix} (I \oplus U^\dagger)(I \oplus V), \tag{2.6}$$

where $U, V \in SO(3)$ correspond to physical unitaries in $SU(2)$.

The maximum singular value of a matrix $\mathcal{M}$ is given by

$$\lambda_{max}(\mathcal{M}) = \max_{\{u,v:\|u\|_2,\|v\|_2\leq 1\}} v^\dagger \mathcal{M} u \tag{2.7}$$

$$\geq \max_{\{v:\|v\|_2\leq 1, j\}} v^\dagger \mathcal{M} e_j \tag{2.8}$$

$$= \max_j \|\mathcal{M} e_j\|_2, \tag{2.9}$$

where u and v are vectors, and $\|Me_j\|_2$ is the Euclidean norm of the j^{th} column of $\mathcal{M}$, so that we can conclude that $1 \geq \lambda_{max}(\mathcal{N}_u) \geq \|\mathcal{N}_u e_j\|_2 \forall j$. Then,

$$1 \geq \|\mathcal{N}_u e_j\|_2^2 = \sum_{\sigma \in \mathbb{P}\backslash I} |(\mathcal{N}_u)_{\sigma,\tau}|^2 \tag{2.10}$$

$$\geq (1-3r)^2 + \sum_{\sigma \neq \tau} |E_{\sigma,\tau}|^2 \tag{2.11}$$

$$\geq (1 - 6r + 9r^2) + |E_{\sigma\neq\tau,\tau}|^2, \tag{2.12}$$

where $\tau \in \mathbb{P}\backslash I$ is the Pauli indexed by j, and

$$|E_{\sigma\neq\tau,\tau}| \leq \sqrt{6r - 9r^2}. \tag{2.13}$$

□

Corollary 15. *For any single-qubit Markovian noise channel with infidelity $r \leq 1/3$,*

$$\mathcal{E}_{\sigma,\sigma'} \leq \sqrt{6r} \tag{2.14}$$

where $\sigma, \sigma' \in (\mathbb{P}\backslash I)/\sqrt{2}$.

The bound on the off-diagonal elements of $\mathcal{E}$ can be further tightened by considering unitarity.

Proof. This follows directly from lemma 14. □

Theorem 16. *For any single-qubit Markovian noise channel with infidelity $r \leq 1/3$ and unitarity u,*

$$\mathcal{E}_{\sigma,\sigma'} \leq \min\{\sqrt{6r - 9r^2}, \sqrt{3u - 3(1-2r)^2}\} \tag{2.15}$$

where $\sigma, \sigma' \in (\mathbb{P}\backslash I)/\sqrt{2}$.

Proof. The first expression in the minimization comes directly from lemma 14. The second term can be derived using the following inequality from [19, eq. 70]

$$3(1-2r)^2 \leq \sum_{\sigma} (\mathcal{N}_u)^2_{\sigma,\sigma} \tag{2.16}$$

and the fact that $\|\mathcal{N}_u\|_F \leq 3u$, where $\|\cdot\|_F$ denotes the Frobenius norm, from [4, Prop. 3]. □

2.2 Scaling of Process Matrix Entries with Error Correction

In this section, we examine the scaling of off-diagonal elements of the effective logical process matrix after syndrome measurement and recovery operations are applied, in order to conclude that the use of quantum error correcting codes decoheres noise, that is, causes the effective noise to converge to a Pauli channel. It is worth noting that the results presented in this section can be applied to the case where no recovery operations are applied.

2.2.1 Separable Noise

Theorem 17. *For an $[\![n, k, d]\!]$ code, after syndrome measurement, the off-diagonal elements of the logical process matrix for a local physical noise process scale as*

$$\mathcal{N}(m)_{\sigma,\sigma'} \in \mathcal{O}(r_{phys}^{d/2}), \tag{2.17}$$

where $r_{phys} = max_j r(\mathcal{N}^{(j)})$*, and we define a local noise process as one which can be expressed as* $\mathcal{N} = \bigotimes_{j\in\mathbb{Z}_n} \mathcal{N}^{(j)}$.

Proof. From eq. (1.86), the effective logical process matrix after syndrome m is measured is given by

$$\overline{\mathcal{N}}_{\sigma,\sigma'}(m) = \frac{1}{|\mathbb{S}|} \sum_{S,S'\in\mathbb{S}} \nu(S|m)\chi(S\overline{\sigma})\chi(S'\overline{\sigma}') \prod_{j\in\mathbb{Z}_n} \mathcal{N}^{(j)}_{(S\overline{\sigma})_j,(S'\overline{\sigma}')_j}. \tag{2.18}$$

By definition, $S\overline{\sigma}$ and $S'\overline{\sigma}'$ must differ on at least d qubits for a distance d stabilizer code for any $\sigma \neq \sigma'$. By corollary 15, then,

$$\overline{\mathcal{N}}_{\sigma,\sigma'}(m) \leq |\mathbb{S}|(6r)^{d/2}. \tag{2.19}$$

From the bounds on the other elements of the process matrix given by lemma 14, $r^{d/2}$ is the lowest order term that will arise in the calculation of the off-diagonals of the logical process matrix. □

Theorem 18. *Applying a recovery operation* $R \in \mathbb{P}_n$ *will not change the magnitude of the per-syndrome process matrix entries.*

Proof. The process matrix for any Pauli operator is diagonal (recall eq. (1.101)), with $\mathcal{N} = \pm 1$, so applying any Pauli recovery process will only change the sign of the process matrix elements. □

Corollary 19. *The off-diagonal elements of the effective logical process matrix for an* $[\![n, k, d]\!]$ *code undergoing separable physical noise,* $\bigotimes_{j\in\mathbb{Z}_n} \mathcal{N}^{(j)}$*, with full error correction using Pauli recovery operators will scale as*

$$\mathcal{N}(m)_{\sigma,\sigma'} \in \mathcal{O}(r_{phys}^{d/2}), \tag{2.20}$$

where $r_{phys} = max_j r(\mathcal{N}^{(j)})$.

Proof. Corollary 19 follows directly from theorem 17 and theorem 18. □

In theorem 17, we showed that errors on the off-diagonal elements of the process matrix are suppressed exponentially with code distance. In order to conclude that errors decohere with error correction, we must argue that the diagonal elements of the process matrix are not suppressed proportionally; if error correction decoheres errors, the scaling of the off-diagonal elements of the error matrix should be less than the square root of the diagonals.

The contributions of errors on subsets of qubits on the noise channel are discussed in more detail in section 2.5, but for the purposes of this section, the following suffices. We can express the noise as a sum over errors acting on subsets of qubits as

$$\mathcal{N} = \sum_{l \subseteq \mathbb{Z}_n} \mathcal{J}(l), \tag{2.21}$$

where $\mathcal{J}(l)$ is an error acting only on the qubits indexed by l. Then, we can write the effective noise after syndrome m is measured and recovery R_m is applied as

$$\mathcal{N}(R_m)_{\sigma,\sigma'} = \sum_{l \subseteq \mathbb{Z}_n} \mathcal{N}(R_m, l)_{\sigma,\sigma'}, \tag{2.22}$$

where

$$\mathcal{N}(R_m, l)_{\sigma,\sigma'} = \frac{1}{p(m)} \sum_{S,S' \in \mathbb{S}} \eta(S\overline{\sigma}, R_m)\chi(S\overline{\sigma})\chi(S'\overline{\sigma}') \prod_{j \in l} \mathcal{J}(l)^{(j)}_{(S\overline{\sigma})_j,(S'\overline{\sigma}')_j}. \tag{2.23}$$

For any $[\![n, k, d]\!]$ code, there will exist an un-correctable error with weight at most $\lceil d/2 \rceil$, acting on qubits indexed by $v \subset \mathbb{Z}_n$, which will contribute a term to the expression given in eq. (2.22). The contribution of this term to the diagonal elements of $\mathcal{N}(R_m)$ is given by

$$\mathcal{N}(R_m, v)_{\sigma,\sigma} = \frac{1}{p(m)} \sum_{S \in \mathbb{S}} \eta(S\overline{\sigma}, R_m)\chi(S\overline{\sigma})^2 \prod_{j \in v} \mathcal{J}(v)^{(j)}_{(S\overline{\sigma})_j,(S\overline{\sigma})_j} \tag{2.24}$$

$$= \frac{1}{p(m)} \sum_{S \in \mathbb{S}} \eta(S\overline{\sigma}, R_m) \prod_{j \in v} \mathcal{J}(v)^{(j)}_{(S\overline{\sigma})_j,(S\overline{\sigma})_j}, \tag{2.25}$$

where the $\chi(\cdot)$ are omitted in the second line because $\chi(S\overline{\sigma}) = \pm 1$ and $(\pm 1)^2 = 1$[1]. From eq. (2.1c), this term will scale at worst proportionally to $r^{|u|} = r^{\lceil d/2 \rceil}$. Recalling that the off-diagonals scale as $r^{d/2}$ post-error correction, and that absent error correction, the diagonals are approximately the square of the off-diagonals (and both are ≤ 1) from lemma 14, we can conclude that error correction decoheres noise, and that with increasing d, noise becomes more Pauli.

This decoherence can be attributed to the syndrome measurements, rather than the recovery operations; syndrome measurements have the effect of removing some terms in the expansion of the state, as shown below. The encoded state can be expressed as

$$\overline{\rho} = \sum_{\overline{\sigma} \in \mathbb{L}} c(\overline{\sigma}) S\overline{\sigma} = \sum_{\overline{\sigma} \in \mathbb{L}} c(\overline{\sigma}) \Pi_0 \overline{\sigma}. \tag{2.26}$$

After exposure to some noise, the state is not necessarily in the codespace,

$$\mathcal{N}[\overline{\rho}] = \sum_{P \in \mathbb{P}_n} c'(P) P, \tag{2.27}$$

where

$$c'(P) = \sum_{\substack{S \in \mathbb{S} \\ \sigma \in \mathbb{P}}} c(\overline{\sigma}) \prod_{j \in \mathbb{Z}_n} \mathcal{N}_{P_j, (S\overline{\sigma})_j}. \tag{2.28}$$

After syndrome measurement projects onto the cospace associated with syndrome m, the state is given by

$$\Pi_m \mathcal{N}[\overline{\rho}] \Pi_m = \sum_{P \in \mathbb{P}_n} c'(P) \Pi_m P \Pi_m, \tag{2.29}$$

where the Π_m annihilate any $P \in \mathbb{P}_n$ that is not of the form $S'\overline{\sigma}'$. The state after syndrome measurement can then be expressed as

[1] The phase on $S\overline{\sigma}$ relative to an element of the Pauli group will always be ± 1 because S and $\overline{\sigma}$ are Hermitian operators and so their product must also be a Hermitian operator.

$$\Pi_m \mathcal{N}[\overline{\rho}]\Pi_m = \sum_{\substack{S,S'\in\mathbb{S}\\ \sigma,\sigma'\in\mathbb{P}}} c'(S'\overline{\sigma}')S'L' \tag{2.30}$$

$$= \sum_{S\overline{\sigma},S'\overline{\sigma}'} c(\overline{\sigma}) \prod_{j\in\mathbb{Z}_n} \mathcal{N}_{(S'\overline{\sigma}')_j,(S\overline{\sigma})_j} S'\overline{\sigma}'. \tag{2.31}$$

Terms appearing in the sum in eq. (2.27) that do not have the form $S'\overline{\sigma}'$ arise predominantly due to contributions from coherent errors[2]. Thus, we can qualitatively conclude that the suppression of coherent errors is achieved via syndrome measurement.

2.2.2 General Noise

General, potentially correlated, noise can be written in the form

$$\mathcal{N} = \sum_{\alpha} p_\alpha \bigotimes_{j\in\mathbb{Z}_n} \mathcal{N}^{(\alpha,j)}, \tag{2.32}$$

where p_α gives the probability of occurence for the separable noise $\bigotimes_{j\in\mathbb{Z}_n} \mathcal{N}^{(\alpha,j)}$, analogous to the definition of mixed states given by eq. (1.3).

By linearity, the analysis of relative scaling of the elements of diagonal to off-diagonal elements of the effective logical noise for a separable noise process should extend directly to the more general case of non-separable noise. It can therefore be concluded that for any general noise process, error correction will decohere the noise.

The parameter that performs the role analogous to the single qubit infidelity, r, in the case of more general noise remains unclear, and finding such a parameter is an open problem.

2.3 Choosing Recovery Operations with Infidelity

In section 2.2 we demonstrated that with increasing code distance, the effective logical noise should converge to a Pauli channel, though contributions from the coherent part of the physical noise will have a non-negligible effect on this final channel. For this reason, it is appropriate to use fidelity as a metric of error rates at the logical level for error correcting

[2] Consider the effect of applying a coherent rotation to a single qubit Pauli.

codes with large distance, as fidelity effectively quantifies the contributions from the Pauli part of the noise. Further, the discrepancies between diamond distance and fidelity should become negligible as code distance increases and the noise approaches a Pauli channel. The use of fidelity rather than another metric such as the diamond distance to quantify errors post-correction in order to select recovery operations is convenient because the fidelity is a linear function, so we can optimize the fidelity independently for each error syndrome, as noted in [10]. In order to use the diamond distance or another non-linear metric, we would have to optimize simultaneously over all possible combinations of recovery operators.

The selection of recovery operations using infidelity is convenient for simulations, because by *eq.* (1.46) the fidelity of a noise process only depends on the trace of the process matrix, which significantly reduces the number of terms required relative to calculating the full process matrix. Further, this approach has already been validated via calculation of process matrices to produce better thresholds than the traditional symmetric or CSS recovery protocol [10]. In CSS recovery, a lowest weight operator is associated with each error syndrome, with preference given to recovery operators with weight on X and/or Z rather than Y.

2.4 Approximating the Logical Noise

Calculating the exact process matrix for an $[\![n, k, d]\!]$ stabilizer code as given by eq. (1.100) requires a sum over $12(n-k)^3$ terms[3]. As such, it is infeasible to evaluate the exact logical noise for any but the smallest codes. In this section, we present the Pauli twirl approximation (PTA) of a logical process matrix, and show how to make corrections to the PTA up to a specified order in r.

2.4.1 Pauli Twirl Approximation

Applying a Pauli twirl (see section 1.2.1) at the physical level produces a Pauli channel, for which the contributing physical noise on each qubit is diagonal, that is, $\mathcal{N}^{(j)}$ is diagonal $\forall j$. To calculate this channel, it is sufficient to allow $\mathcal{N}^{(j)}_{\sigma,\tau} = 0 \; \forall \sigma \neq \tau$ and calculate $\mathcal{N}^{(j)}_{\sigma,\sigma}$ as normal, so that the PTA of the physical process matrices are diagonal.

[3] The first row of the process matrix is fixed by the trace preserving condition. The remaining 12 terms each require a sum over the set of recovery operations and two sums over the set of stabilizers, for which $|\mathbb{R}| = |\mathbb{S}| = n - k$.

If we apply a Pauli twirl at the logical level, we get a similar result, with $\overline{\mathcal{N}}_{\sigma,\tau} = 0 \; \forall \sigma \neq \tau$, and

$$\langle \overline{\mathcal{N}}_{\sigma,\sigma} \rangle = \frac{1}{|\mathbb{S}|} \sum_{R \in \mathbb{R}, S \in \mathbb{S}} \eta(R,S) \chi(S\overline{\sigma}) \chi(S\overline{\sigma}) \prod_{j \in \mathbb{Z}_n} \mathcal{N}^{(j)}_{(S\overline{\sigma})_j, (S\overline{\sigma})_j} \tag{2.33}$$

$$= \frac{1}{|\mathbb{S}|} \sum_{R \in \mathbb{R}, S \in \mathbb{S}} \eta(R,S) \prod_{j \in \mathbb{Z}_n} \mathcal{N}^{(j)}_{(S\overline{\sigma})_j, (S\overline{\sigma})_j}, \tag{2.34}$$

$\forall \sigma \in \mathbb{P}$ because $\chi(S\overline{\sigma}) = \pm 1$. This approximation only requires a sum over $3(n-k)^2$ terms, thus producing a significant reduction in computational complexity.

Typically, simulations rely on Pauli twirling at the physical level in order to simplify the calculations required. Deviation from this approximation has been demonstrated [34, 38], though on average, logical noise appears approximately Pauli. This deviation is explicable as the contribution of the coherent part of the physical noise to the diagonal of the effective logical noise, so that applying the Pauli twirl at the logical level should provide a more accurate approximation of the effective logical noise.

2.4.2 Higher order corrections to the PTA

We now derive corrections to the PTA up to a specified order, w, in r. Let eq. (2.34) denote the 0^{th} order term of the exact noise, so that for a recovery operation R,

$$\overline{\mathcal{N}}(R)^{(0)}_{\sigma,\sigma} = \frac{1}{|\mathbb{S}|} \sum_{S \in \mathbb{S}} \eta(R,S) \prod_{j \in \mathbb{Z}_n} \mathcal{N}^{(j)}_{(S\overline{\sigma})_j, (S\overline{\sigma})_j}. \tag{2.35}$$

This is equivalent to applying a Pauli twirl at the physical level. Using lemma 14, each term of the right-hand-side of eq. (1.100) will contribute at most $\mathcal{O}(r^{\Gamma(S\overline{\sigma}, S'\overline{\sigma}')/2})$, where

$$\Gamma(A,B) = |\{j : A_j B_j = -B_j A_j\}| \tag{2.36}$$

$$+ \infty |\{j : A_j \neq B_j = I\}| \tag{2.37}$$

$$+ 2|\{j : B \neq A = I\}|. \tag{2.38}$$

Equation (2.36) comes from eq. (2.1d), eq. (2.37) is from eq. (2.1a), and eq. (2.38) comes from eq. (2.1b) and eq. (2.1c) and effectively counts the number of indices on which the

input operators commute and anticommute, with or without acting on that index with an identity operator.

The r^w correction to the PTA is then given by

$$\overline{\mathcal{N}}(R)^{(w)}_{\sigma,\sigma'} = \frac{1}{|\mathbb{S}|} \sum_{S,S' \in \mathbb{S}:\Gamma(S\overline{\sigma},S'\overline{\sigma}')=w} \eta(R,S)\chi(S\overline{\sigma})\chi(S'\overline{\sigma}') \prod_{j\in\mathbb{Z}_n} \mathcal{N}^{(j)}_{(S\overline{\sigma})_j,(S\overline{\sigma}')_j}. \tag{2.39}$$

To calculate the effective logical process matrix up to order w, we then use eq. (2.39) as follows

$$\overline{\mathcal{N}}(R)_{\sigma,\sigma'} \approx \sum_{j\in\mathbb{Z}_{w+1}} \overline{\mathcal{N}}(R)^{(j)}_{\sigma,\sigma'}. \tag{2.40}$$

This derivation generalizes trivially to the approximation of noise after syndrome measurement but without the application of recovery operations.

2.5 Contributions from Subsets of Qubits

In the event that some qubits are known to undergo a significantly more severe noise process than others, it is useful to consider the effective logical noise arising from the noise acting on only a subset of physical qubits. This section derives an equation for use in such a case, first for the PTA, and then for more general noise.

2.5.1 The PTA from a Subset of Qubits

Recalling that we defined $\mathcal{E} = |\mathcal{I} - \mathcal{N}|$ in order to quantify errors on elements of the process matrix in section 2.1, we substitute $\mathcal{N}^{(j)} = \mathcal{I} + \mathcal{E}^{(j)}$ into eq. (2.34) and expand to get

$$\overline{\mathcal{N}}(R)_{\sigma,\sigma} = \sum_{l\subseteq\mathbb{Z}_n} \overline{\mathcal{E}}(R)^{(l)}_{\sigma,\sigma}, \tag{2.41}$$

where

$$\overline{\mathcal{E}}(R)_{\sigma,\sigma} = \frac{1}{|\mathbb{S}|}\sum_{S\in\mathbb{S}}\eta(R,S)\prod_{j\in l}\mathcal{E}_{(S\overline{\sigma})_j,(S\overline{\sigma})_j}\prod_{j\notin l}\mathcal{I}_{(S\overline{\sigma})_j,(S\overline{\sigma})_j} \tag{2.42}$$

$$= \frac{1}{|\mathbb{S}|}\sum_{S\in\mathbb{S}}\eta(R,S)\prod_{j\in l}\mathcal{E}_{(S\overline{\sigma})_j,(S\overline{\sigma})_j}. \tag{2.43}$$

Let $\mathbb{S}_l \subseteq \mathbb{S}$ be the subgroup of $\mathbb{S}$ that acts trivially on all elements indexed by l, $\mathbb{S}_l^{\|} \subseteq \mathbb{S}$ be the set of operators which commute with every element in $\mathbb{S}_l$, and $\mathbb{S}_l^{\perp} \subseteq \mathbb{S}$ be the complementary set. Any $R \in \mathbb{S}_l^{\perp} \cap \mathbb{R}$ anticommutes with exactly half of the elements of $\mathbb{S}_l$, so that any recovery operator which corrects errors outside of l does not contribute to $\overline{\mathcal{E}}^{(l)}$. Then,

$$\overline{\mathcal{N}}_{\sigma,\sigma} = \sum_{R\in\mathbb{S}_l^{\|}\cap\mathbb{R}}\overline{\mathcal{N}}(R)_{\sigma,\sigma} \tag{2.44}$$

$$= \sum_{\substack{l\subseteq\mathbb{Z}_n \\ R\in\mathbb{S}_l^{\|}\cap\mathbb{R}}}\overline{\mathcal{E}}(R)^{(l)}_{\sigma,\sigma}, \tag{2.45}$$

where

$$\overline{\mathcal{E}}(R)^{(l)}_{\sigma,\sigma} = \frac{1}{|\mathbb{S}|}\sum_{\substack{S\in\mathbb{S} \\ U\in\mathbb{S}/\mathbb{S}_l}}\eta(R,SU)\prod_{j\in l}\mathcal{E}^{(j)}_{(U\overline{\sigma})_j} \tag{2.46}$$

$$= \frac{1}{|\mathbb{S}/\mathbb{S}_l|}\sum_{U\in\mathbb{S}/\mathbb{S}_l}\eta(R,U)\prod_{j\in l}\mathcal{E}^{(j)}_{(U\overline{\sigma})_j}. \tag{2.47}$$

2.5.2 Off-Diagonals from a Subset of Qubits

Using a procedure similar to that used to derive eq. (2.47), we arrive at an expression for the off-diagonal elements of the effective logical process matrix arising from noise contributions from a subset of qubits,

$$\overline{\mathcal{N}}_{\sigma,\sigma'} = \sum_{\substack{l\subseteq\mathbb{Z}_n \\ R\in\mathbb{S}_l^{\|}\cap\mathbb{R}}}\overline{\mathcal{E}}(R)^{(l)}_{\sigma,\sigma'}, \tag{2.48}$$

where

$$\overline{\mathcal{E}}(R)^{(l)}_{\sigma,\sigma'} = \frac{1}{|\mathbb{S}/\mathbb{S}_l|} \sum_{\substack{S,S'\in\mathbb{S}_l \\ U,V\in\mathbb{S}/\mathbb{S}_l}} \eta(R,U)\chi(S\overline{\sigma})\chi(S'\overline{\sigma}') \prod_{j\in l} \mathcal{E}_{(U\overline{\sigma})_j,(V\overline{\sigma})_j} \prod_{j\notin l} \delta(S_j\overline{\sigma}_j, S'_j\overline{\sigma}'_j). \tag{2.49}$$

Theorem 20. *Any physical noise process which acts on fewer than d qubits will produce Pauli noise at the logical level*[4]*.*

Proof. By the definition of the code distance, we know that $S\overline{\sigma}$ and $S'\overline{\sigma}'$ differ on at least d qubits for any $S, S' \in \mathbb{S}, \sigma \neq \sigma' \in \mathbb{P}$. We can therefore neglect any terms with $|l| < d$ in eq. (2.49), which implies that any noise process which acts on fewer than d qubits will have $\mathcal{N}_{\sigma,\tau} = 0\ \forall \sigma \neq \tau$, thus producing Pauli logical noise. □

[4] This statement holds for noise with or without the application of syndrome measurements and/or recovery operations.

Chapter 3

Quantum Error Correction: What Does the Noise Look Like and When Does it Look the Same Under Different Conditions?

Distinct recovery operations will not always produce distinct effective noise maps [10, 39]. It is useful to know when a particular recovery operator will produce the same effective noise as another because if we have this information a priori, it becomes unnecessary to do the full calculation for both recovery maps as we know the results of one from the other. This knowledge can drastically reduce the computational cost of calculating the effective process matrix averaged over syndromes, and can remove recovery operators from consideration in the selection of recovery operations, thus simplifying that procedure. Ref. [39] showed that for an effective logical noise process that can be expressed as a unitary channel[1], it is often possible to find Clifford operations which leave the effective logical noise invariant when they act on the recovery operations, and gave examples for the 5- and 7-qubit codes. This section provides a generalization of that result, which was obtained independently prior to the publication of ref. [39]. We present conditions for equivalent noise under different recovery operations for general noise and an arbitrary stabilizer code.

Theorem 21. *The effective logical noise in a quantum error correcting code is equivalent for any two recovery operations $R, R' \in \mathbb{R}$ for which there exist unitary channels, $\mathcal{U}, \mathcal{V}$, with $[\mathcal{U}, \mathcal{N}] = 0$, such that $\mathcal{U}^\dagger \mathcal{R} \mathcal{V} = \mathcal{R}'$ and which leave $\Pi_{m_0} \overline{\sigma}$ invariant $\forall \sigma \in \mathbb{P}$.*

Proof. Following a derivation similar to that used in **??** 18: *Effective Noise with Full Error*

[1] They thus restrict attention noise that can be expressed in terms of a single Kraus operator.

Correction, we can write the effective logical noise under full error correction conditioned on recovery operation, R, as

$$\overline{\mathcal{N}}(R)_{\sigma,\sigma'} = \frac{1}{2^n|\mathbb{S}|}\sum_{S,S'\in\mathbb{S}} \langle\langle S\overline{\sigma}|\mathcal{R}^\dagger\mathcal{N}|S'\overline{\sigma}'\rangle\rangle \tag{3.1}$$

$$= \frac{1}{2^k}\langle\langle \Pi_{m_0}\overline{\sigma}|\mathcal{R}^\dagger\mathcal{N}|\Pi_{m_0}\overline{\sigma}'\rangle\rangle \tag{3.2}$$

Assuming the existence of channels $\mathcal{U}$ and $\mathcal{V}$ which leave $\Pi_{m_0}\overline{\sigma}$ invariant $\forall\sigma\in\mathbb{P}$, we can re-write eq. (3.2) as

$$\overline{\mathcal{N}}(R)_{\sigma,\sigma'} = \frac{1}{2^k}\langle\langle \Pi_{m_0}\overline{\sigma}|\mathcal{V}^\dagger\mathcal{R}^\dagger\mathcal{N}\mathcal{U}|\Pi_{m_0}\overline{\sigma}'\rangle\rangle, \tag{3.3}$$

because $\mathcal{U}$ and $\mathcal{V}$ leave $\Pi_{m_0}\overline{\sigma}$ invariant, and because the input and output states are both on the codespace. With $[\mathcal{U},\mathcal{N}]=0$, this is equivalent to

$$\overline{\mathcal{N}}(R)_{\sigma,\sigma'} = \frac{1}{2^k}\langle\langle \Pi_{m_0}\overline{\sigma}|\mathcal{V}^\dagger\mathcal{R}^\dagger\mathcal{U}\mathcal{N}|\Pi_{m_0}\overline{\sigma}'\rangle\rangle. \tag{3.4}$$

Comparing eq. (3.4) to eq. (3.2), it is clear that a recovery operator, $\mathcal{R}'$, for which $\mathcal{R}'^\dagger = \mathcal{V}^\dagger\mathcal{R}^\dagger\mathcal{U}$ will produce the same effective logical noise as $\mathcal{R}$. This is equivalent to $\mathcal{R}' = \mathcal{U}^\dagger\mathcal{R}\mathcal{V}$. □

Corollary 22. *Any permutation operator which leaves $\Pi_0\overline{\sigma}$ invariant $\forall\sigma\in\mathbb{P}$ can be used to generate sets of equivalent recovery operations for a given code.*

Proof. A permutation operator can be re-written as a product of transpose operations, each of which exchanges two elements [40]. A transpose operation serves the same role in a quantum system as a SWAP gate, which exchanges the positions of two qubits. Because the SWAP gate is a unitary operation, we can re-write any permutation operator as a product of SWAP gates, ie as a unitary operation. Replacing $\mathcal{V}^\dagger$ from theorem 21 with this permutation and $\mathcal{U}$ with the identity channel, corollary 22 follows as a direct consequence of theorem 21. □

3.1 Examples of Symmetries in Common Error Correcting Codes

This section presents operators which partition sets of recovery operations into equivalence classes for the 3 qubit quantum repetition code, the 5-qubit code, the Steane code, and the Shor code.

3.1.1 Equivalent Effective Noise in the 3 Qubit Repetition Code

In the 3 qubit repetition code, the (0 1 2) operator leaves $\Pi_0\overline{\sigma}$ invariant $\forall\sigma \in \mathbb{P}$[2]. The (0 1 2) operator can be equivalently expressed as a product of $\text{SWAP}_{0,1}$ and $\text{SWAP}_{1,2}$. As such, any subsets of the recovery operators which are closed under these operations will produce equivalent logical noise. Noting the set of errors for which this code is designed, the typical set of recovery operations selected for the 3 qubit repetition code is $\mathbb{R} = \{I^{\otimes 3}, XII, IXI, IIX\}$. Observing the effects of the aforementioned SWAP gates on these recovery operations, it is clear that $\overline{\mathcal{N}}(XII) = \overline{\mathcal{N}}(IXI) = \overline{\mathcal{N}}(IIX)$.

This symmetry was observed by Huang *et.al* in ref. [39] for the specific case of a rotation about the z-axis, though no operator was specified to generate the symmetry.

3.1.2 Equivalent Effective Noise in the 5 Qubit Code

Ref. [39] showed the symmetry presented in this section; we restate it here as it pertains to general noise in the 5 qubit code, and we extend the analysis to a few cases of non-symmetric recovery. The $\Pi_0\overline{\sigma}$ operator of the 5 qubit code is left invariant $\forall\overline{\sigma} \in \mathbb{P}$ by the cyclic permutation[3] (0 1 2 3 4). This permutation operator can equivalently be expressed as a product of $\text{SWAP}_{0,1}$, $\text{SWAP}_{1,2}$, $\text{SWAP}_{2,3}$, $\text{SWAP}_{3,4}$, and $\text{SWAP}_{4,0}$. For the popular symmetric decoder, then, it is clear that $\overline{\mathcal{N}}(R)$ is the same for any single qubit X recovery operator, that any single qubit Z recovery operator will produce equivalent logical noise, and that the single qubit Y recovery operators are an equivalence class as well.

The Z-only recovery set containing the trivial recovery operation, all single qubit Z operators, and all 2-qubit Z operators is partitioned into 4 equivalence classes by (0 1 2 3 4),

[2] Note that this operator is not unique; there are others which leave $\Pi_0\overline{\sigma}$ invariant $\forall\overline{\sigma} \in \mathbb{P}$. This is true for all codes explored in this section.

[3] We do not include the additional permutation presented in ref. [39] as it does not decrease the number of equivalence classes for any of the decoders explored in this section.

with representative elements $IIIII$, $ZIIII$, $ZZIII$, and $ZIZII$. An X-only or Y-only recovery set can be similarly partitioned.

3.1.3 Equivalent Effective Noise in the 7 Qubit Steane Code

The recovery operations of the 7 qubit Steane code can be partitioned by the cyclic permutations $(4\,5)(6\,7)$ and $(1\,4\,2)(3\,5\,6)$[4]. A similar permutation was achieved by Huang *et. al* in ref. [39] using a set of 4 permutation operators. Ref. [39] only explores the set of recovery operations we refer to below as Calderbank-Shor-Steane recovery; we demonstrate equivalence classes for an additional, symmetric, set of recovery operations, and note that their partitioning extends to the case of non-unitary noise.

A[5] set of symmetric recovery operations for the Steane code consists of the trivial error, all single-qubit Pauli errors, and a subset of 2-qubit Pauli errors. The equivalence classes generated by the permutation operators given above are presented in table 3.1.

Class	Recovery Operators
1	$I^{\otimes 7}$
2	Weight 1 X errors
3	Weight 1 Y errors
4	Weight 1 Z errors
5	$ZXIIIII$, $XZIIIII$, $ZIIXIII$, $XIIZIII$, $ZIIIIIX$, $XIIIIIZ$, $IZIXIII$, $IXIZIII$, $IZIIIIX$, $IXIIIIZ$, $IIIZIIX$, $IIIXIIZ$, $IIZIXII$, $IIZIIXI$, $IIXIZII$, $IIIIZXI$, $IIXIIZI$, $IIIIXZI$
6	$YXIIIII$, $XYIIIII$, $YIIXIII$, $XIIYIII$, $YIIIIIX$, $XIIIIIY$, $IYIXIII$, $IXIYIII$, $IYIIIIX$, $IXIIIIY$, $IIIYIIX$, $IIIXIIY$
7	$YZIIIII$, $ZYIIIII$, $YIIZIII$, $ZIIYIII$, $YIIIIIZ$, $ZIIIIIY$, $IYIZIII$, $IZIYIII$, $IYIIIIZ$, $IZIIIIY$, $IIIYIIZ$, $IIIZIIY$

Table 3.1: Equivalence classes for a symmetric decoder in the 7 qubit Steane code.

[4] Like permutation operators specified for other codes, these operators are not unique. Two are given for this code because together, they partition the sets of recovery operations explored into a minimal set of equivalence classes. The same convention is followed in specifying permutations for the 9 qubit Shor code.

[5] In codes other than the 5 qubit code, there are often syndromes which have more than one error with the minimal weight; in such cases, a recovery operation is chosen arbitrarily from the set of minimum weight errors for that syndrome. As such, a set of symmetric recovery operations is generally not unique.

Another popular set of recovery operations for the Steane code is the Calderbank-Shor-Steane (CSS) recovery: the set containing the trivial error, all single qubit Pauli errors, and all weight 2 errors with 1 X error and 1 Z error. The given permutation operators partition this set of recovery operations into 5 equivalence classes, as demonstrated in ref. [39] for unitary noise, with all recovery operators of a given weight of the same type of Pauli in the same class[6].

These permutation operators group any set of recovery operations with weight 2 acted upon by the same Pauli operators into the same equivalence class.

The equivalence classes of recovery operations explored for the Steane code in this section resolve an open question posed in [39]; they noted that in [10] we found 7 unique channels, whereas in [39] they only observed 5. Ref. [39] conjectured that this discrepancy was due to their restriction to unitary channels, however, we showed above that the number of equivalence classes is a side effect of the selected recovery protocol.

3.1.4 Equivalent Effective Noise in the 9 Qubit Shor Code

For the 9 qubit Shor code, (4 7)(5 8)(6 9) and (1 4)(2 5)(3 6)(7 8 9) can be used to partition recovery operations into equivalence classes. For a symmetric decoder, these operators generate 12 equivalence classes, specifed in table B.1 of appendix B.

3.2 The Evolution of Depolarizing Noise

This section explores the behaviour of the completely depolarizing channel introduced in section 1.2.1, and in particular, how this noise model behaves in a concatenated 5 qubit or Steane code.

3.2.1 A General Expression for Depolarizing Noise in a QECC

From eq. (1.100), the process matrix for an encoded channel, conditioned on a single syndrome measurement m and the application of the corresponding recovery operator, undergoing depolarizing noise on each physical qubit is given by

[6] This set is also a set of symmetric recovery operations, and is referred to as the symmetric recovery in ref. [39]. In this thesis, we have defined a different set of symmetric recovery operations and because this set focuses on $X-$ and $Z-$type recovery, we label this one CSS.

$$\overline{\mathcal{N}}(R_m)_{\sigma,\sigma'} = \frac{1}{2^k|\mathbb{S}|^2}\sum_{S,S'\in\mathbb{S}} \eta(S\overline{\sigma}, R_m)\langle\langle S\overline{\sigma}|\mathcal{D}^{\otimes n}|S'\overline{\sigma}'\rangle\rangle, \tag{3.5}$$

where $\mathcal{D}$ is the depolarizing channel. Examining the action of the depolarizing channel, we see that it has the following effects on Pauli operators,

$$\mathcal{D}[I] = I \tag{3.6}$$
$$\mathcal{D}[P] = (1-p)A, \ \ \forall A \in \mathbb{P}\backslash I. \tag{3.7}$$

Then,

$$\mathcal{D}_p^{\otimes n}|S'\overline{\sigma}'\rangle\rangle = (1-p)^{w(S'\overline{\sigma}')}|S'\overline{\sigma}'\rangle\rangle, \tag{3.8}$$

where $w(A)$ is the weight of A. Equation (3.5) then becomes

$$\overline{\mathcal{N}}(R_m)_{\sigma,\sigma'} = \frac{1}{2^k|\mathbb{S}|^2}\sum_{S,S'\in\mathbb{S}} \eta(S\overline{\sigma}, R_m)(1-p)^{w(S'\overline{\sigma}')}\langle\langle S\overline{\sigma}|S'\overline{\sigma}'\rangle\rangle \tag{3.9}$$

Expanding $\langle\langle S\overline{\sigma}|S'\overline{\sigma}'\rangle\rangle$,

$$\langle\langle S\overline{\sigma}|S'\overline{\sigma}'\rangle\rangle = 2^n\chi(S\overline{\sigma})\chi(S'\overline{\sigma}')\delta_{(S\overline{\sigma}),(S'\overline{\sigma}')} = 2^n\delta_{(S\overline{\sigma}),(S'\overline{\sigma}')}, \tag{3.10}$$

where the global phases can be neglected because their square will always be 1. Thus,

$$\overline{\mathcal{N}}(R_m)_{\sigma,\sigma} = \frac{1}{|\mathbb{S}|}\sum_{S\in\mathbb{S}} \eta(S\overline{\sigma}, R_m)(1-p)^{w(S\overline{\sigma})}, \tag{3.11}$$

and

$$\overline{\mathcal{N}}(R_m)_{\sigma,\sigma'} = 0, \ \forall\sigma \neq \sigma'. \tag{3.12}$$

3.2.2 A Brief Aside: The Evolution of Pauli Noise

In this section, we derive a general expression for Pauli noise in a QECC.

Parameterizing a Pauli channel as follows,

$$\mathcal{P}[\rho] = (1 - p_x - p_y - p_z)I\rho I + p_x X\rho X + p_y Y\rho Y + p_z Z\rho Z, \tag{3.13}$$

the physical process matrix is

$$\mathcal{P} = \begin{bmatrix} 1 & 0 & 0 & 0 \\ 0 & 1-2(p_y+p_z) & 0 & 0 \\ 0 & 0 & 1-2(p_x+p_z) & 0 \\ 0 & 0 & 0 & 1-2(p_x+p_y) \end{bmatrix}. \tag{3.14}$$

Following a procedure similar to that in section 3.2,

$$\overline{\mathcal{N}}(R_m)_{\sigma,\sigma} = \frac{1}{|\mathbb{S}|}\sum_{S\in\mathbb{S}} \eta(S\overline{\sigma}, R_m)[1-2(p_y+p_z)]^{w_x(S\overline{\sigma})}[1-2(p_x+p_z)]^{w_y(S\overline{\sigma})}[1-2(p_x+p_y)]^{w_z(S\overline{\sigma})}, \tag{3.15}$$

where $w_\sigma(A)$ is the number of qubits in A that are acted upon by σ and $\overline{\mathcal{N}}(R_m)_{\sigma,\sigma'} = 0 \forall \sigma \neq \sigma'$.

3.2.3 Depolarizing Noise in the 5 Qubit Code

This section explores the evolution of depolarizing noise in the 5 qubit code; equivalence classes of recovery operations specific to depolarizing noise are presented, and the behaviour of depolarizing noise in a concatenated 5 qubit code is analysed. An expression for the threshold value of the depolarizing parameter is derived.

Additional Symmetry in the 5 Qubit Code Under Depolarizing Noise

Recalling the form of depolarizing noise (eq. (1.105)),

$$\mathcal{D}_p = \begin{bmatrix} 1 & 0 & 0 & 0 \\ 0 & 1-p & 0 & 0 \\ 0 & 0 & 1-p & 0 \\ 0 & 0 & 0 & 1-p \end{bmatrix}, \tag{3.16}$$

it is apparent that additional symmetry is introduced by applying depolarizing noise because depolarizing noise acts in the same way on X, Y, and Z operators. With this in mind, we wish to find an operator which satisfies the conditions introduced in theorem 21, and which maps between Pauli operators. Let $Q = \sqrt{Z}\sqrt{X}$; the unitary channel $\mathcal{Q}(\rho) = Q\rho Q^\dagger$ maps $X \to Y \to Z \to X$ and leaves I invariant. $Q^{\otimes 5}$ preserves $\mathbb{S}\overline{\sigma}\ \forall \sigma \in \mathbb{P}$. The process matrix representation of $\mathcal{Q}$ is

$$\mathcal{Q} = \begin{bmatrix} 1 & 0 & 0 & 0 \\ 0 & 0 & 0 & 1 \\ 0 & 1 & 0 & 0 \\ 0 & 0 & 1 & 0 \end{bmatrix}, \tag{3.17}$$

and $[\mathcal{Q}, \mathcal{D}_p] = 0$, so $\mathcal{Q}^{\otimes 5}$ satisfies the conditions for $\mathcal{U}$ and $\mathcal{V}$ in theorem 21 when $\mathcal{N} = \mathcal{D}_p^{\otimes 5}$. Following theorem 21, we let $\mathcal{U} = \mathcal{V} = \mathcal{Q}^{\otimes 5}$. Then any recovery maps, $\mathcal{R}$ and $\mathcal{R}'$, for which $\mathcal{R}' = (\mathcal{Q}^\dagger)^{\otimes 5}\mathcal{R}\mathcal{Q}^{\otimes 5}$ will result in the same effective logical noise. The single-qubit mapping, $\mathcal{Q}^\dagger R(i)\mathcal{Q}$, takes $\mathcal{X} \to \mathcal{Z} \to \mathcal{Y} \to \mathcal{X}$, so, in conjunction with the previous result that all single qubit errors of a given type share an equivalence class for the 5 qubit code, we can conclude that the set of single qubit errors forms an equivalence class for the 5 qubit code under depolarizing noise. The channel $\mathcal{Q}^\dagger$ can be expressed in terms of a single Kraus operator, $A_0 = \sqrt{-X}\sqrt{-Z}$.

Hard Decoding in the 5 Qubit Code Under Depolarizing Noise

When depolarizing noise acts on every physical qubit in the $[\![5, 1, 3]\!]$ code, the most effective known recovery protocol[7] is to apply symmetric recovery [10].

The average effective logical channel under symmetric recovery has the following form:

[7] In terms of achieving high average fidelity to the identity and maximizing the threshold limit with concatenation.

$$\langle \overline{\mathcal{N}} \rangle = \begin{bmatrix} 1 & 0 & 0 & 0 \\ 0 & \alpha & 0 & 0 \\ 0 & 0 & \alpha & 0 \\ 0 & 0 & 0 & \alpha \end{bmatrix}, \tag{3.18}$$

where $\alpha = \frac{1}{2}(p-1)^3(3p(p-2)-2)$. Recalling the process matrix for depolarizing noise acting on a single qubit (eq. (1.105)), it is clear that the effective logical noise in the 5 qubit code has a similar form on average. Letting $\alpha = 1 - p_{logical}$ so that we can more clearly see the effective noise dynamics as a depolarizing channel on the logical state,

$$p_{logical} = \frac{1}{2}[15p^2 - 25p^3 + 15p^4 - 3p^5]. \tag{3.19}$$

It is therefore trivial to model depolarizing noise in a concatenated 5 qubit code using symmetric recovery at each level of concatenation; the effective noise at the l^{th} level of concatenation is depolarizing with the noise parameter p^l calculated by recursively applying eq. (3.19), such that

$$p^{(l)} = \frac{1}{2}[15(p^{(l-1)})^2 - 25(p^{(l-1)})^3 + 15(p^{(l-1)})^4 - 3(p^{(l-1)})^5], \tag{3.20}$$

where $p^{(0)} = p$ is the noise parameter of the physical noise. It is clear from this expression that $p^{(l)} \in \mathcal{O}(p^{2l})$ for small p. The noise parameters for the first 5 levels of concatenation are plotted as a function of the physical noise parameter in fig. 3.1.

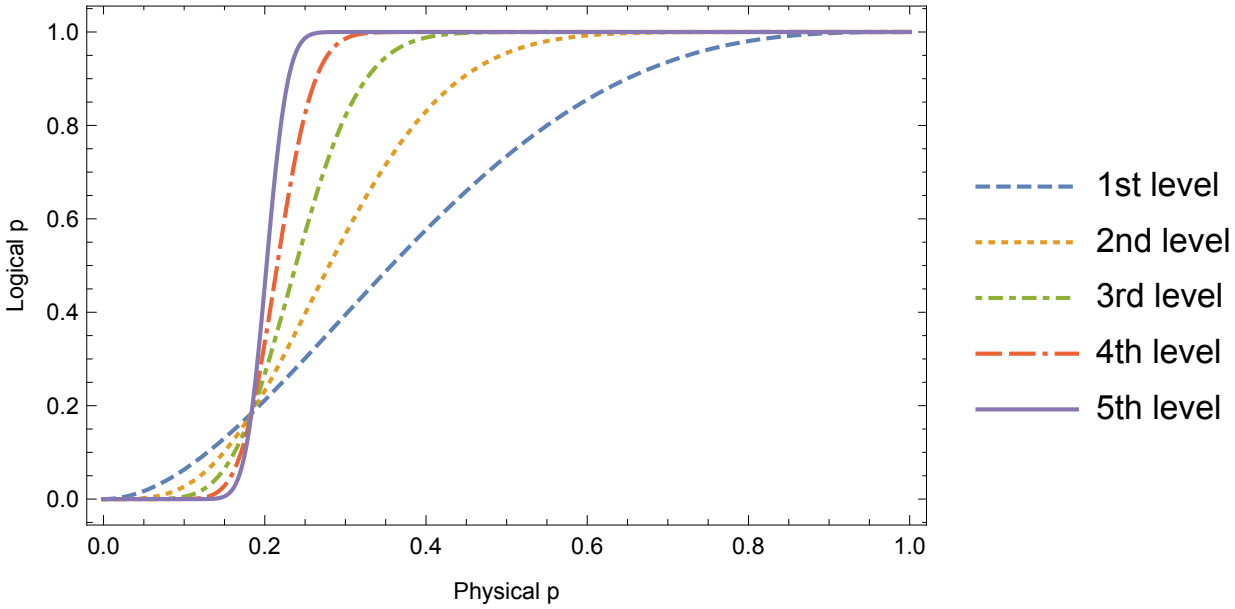

Figure 3.1: Plots of the effective logical noise parameters, $p^{(l)}$, at the l^{th} level of concatenation in the 5 qubit code under depolarizing noise.

Solving eq. (3.19) for when $p = p_{logical}$, we can find the intercept seen in fig. 3.1, which corresponds to the threshold below which depolarizing noise is suppressed by the 5 qubit code with symmetric recovery. The threshold value for the depolarizing noise parameter under these conditions is $p_{threshold} = 1 - \sqrt{2/3}$.

Depolarizing Noise Under Soft Decoding in the 5 Qubit Code

This section presents a soft decoding algorithm tailored to the 5 qubit code under soft decoding. We begin by presenting the general methodology for this algorithm, which can be leveraged for other QECCs, then specialize to a concatenated 5 qubit code under depolarizing noise for performance analysis. The algorithm presented in this section is powerful because it provides a means to simulate soft decoding which is not subject to statistical sampling methods[8]. Further, our algorithm provides a significant increase in performance over the optimal hard decoding method for the 5 qubit code under depolarizing noise, and can, in theory, be similarly leveraged for a similar improvement under different conditions.

[8] For soft decoding algorithms, the simulation method often involves sampling syndrome measurements at each level of concatenation. This approach to threshold estimation is problematic because in the case that the effective logical noise converges for some sampled set of recovery operations for a noise parameter above the threshold value, the threshold estimate could potentially be artificially inflated.

Hard decoding algorithms select recovery operations independently at each level of concatenation, generally by taking the average channel at the previous level of concatenation and feeding it in as the apparent physical noise on each qubit in the next level. Soft decoding is computationally expensive because at each level of concatenation, the noise from the previous levels is not averaged, so there are $2^{(\sum_{i=0}^{l-1} n^i)(n-k)}$ combinations of recovery operations to be considered at the l^{th} level of concatenation. Cumulatively, to concatenate up to the l_{max}^{th} level with general soft decoding, we would need to consider $\sum_{l=1}^{l_{max}} 2^{(\sum_{i=0}^{l-1} n^i)(n-k)}$ terms. In this algorithm, the goal is to leverage the power of soft decoding, while preserving some of the reduction in computational complexity achieved by averaging channels. This is achieved by applying a coarse-graining operation to group channels into bins then averaging over the contents of each bin at every level of concatenation. The algorithm is pictured in fig. 3.2 for the general case with b bins at each level of concatenation, where l_{max} is the number of concatenations applied. Letting $b \to |\mathbb{R}|$ can produce optimal recovery selection, as this is the general soft decoding protocol.

At the first level of concatenation, the normal error correction procedure is followed; the state is encoded, undergoes physical noise, syndrome measurements and recovery operations are applied, and the outcome is 2^{n-k} not-necessarily-distinct channels, one for each syndrome. Then the resultant channels are grouped by some sorting method into b bins of channels and the average channel in each bin is calculated. The subsequent levels see a "physical noise" from the previous level as a permutation of noises from the bins, so that each $\mathcal{N}^{(j)} = \mathcal{N}(\text{bin}_i)$ for some $i \in \mathbb{Z}_b$, where $\mathcal{N}(\text{bin}_i)$ is the average of the channels in the i^{th} bin. This procedure is repeated for every permutation of $\mathcal{N}^{(j)}$s. A syndrome measurement and recovery operation is then applied to each channel, and the coarse graining procedure is repeated so that the same number, b, of channels are fed into the next level as "physical" noise. Thus, for levels $l > 1$, at each level of concatenation there are $b^n \times (2^{n-k})$ channels to consider. The constant scaling makes this implementation feasible to evaluate directly rather than relying on the statistical sampling techniques traditionally used to evaluate the performance of soft decoding algorithms. For l_{max} levels of concatenation, a total of $[(l_{max} - 1)b^n + 1]2^{n-k}$ terms are required.

For the 5 qubit code under depolarizing noise, there are only 2 distinct channels after symmetric recovery at the first level of concatenation. For simplicity, we then let $b = 2$ for binning at the higher levels of concatenation. After re-encoding, the second level undergoes noise in the form of permutations of the two depolarizing noises resulting from the trivial or non-trivial syndrome measurement at the first level. Letting $\mathcal{N}(\text{bin}_0)$ be the noise resulting from trivial recovery and $\mathcal{N}(\text{bin}_1)$ be the noise resulting from non-trivial recovery, we now

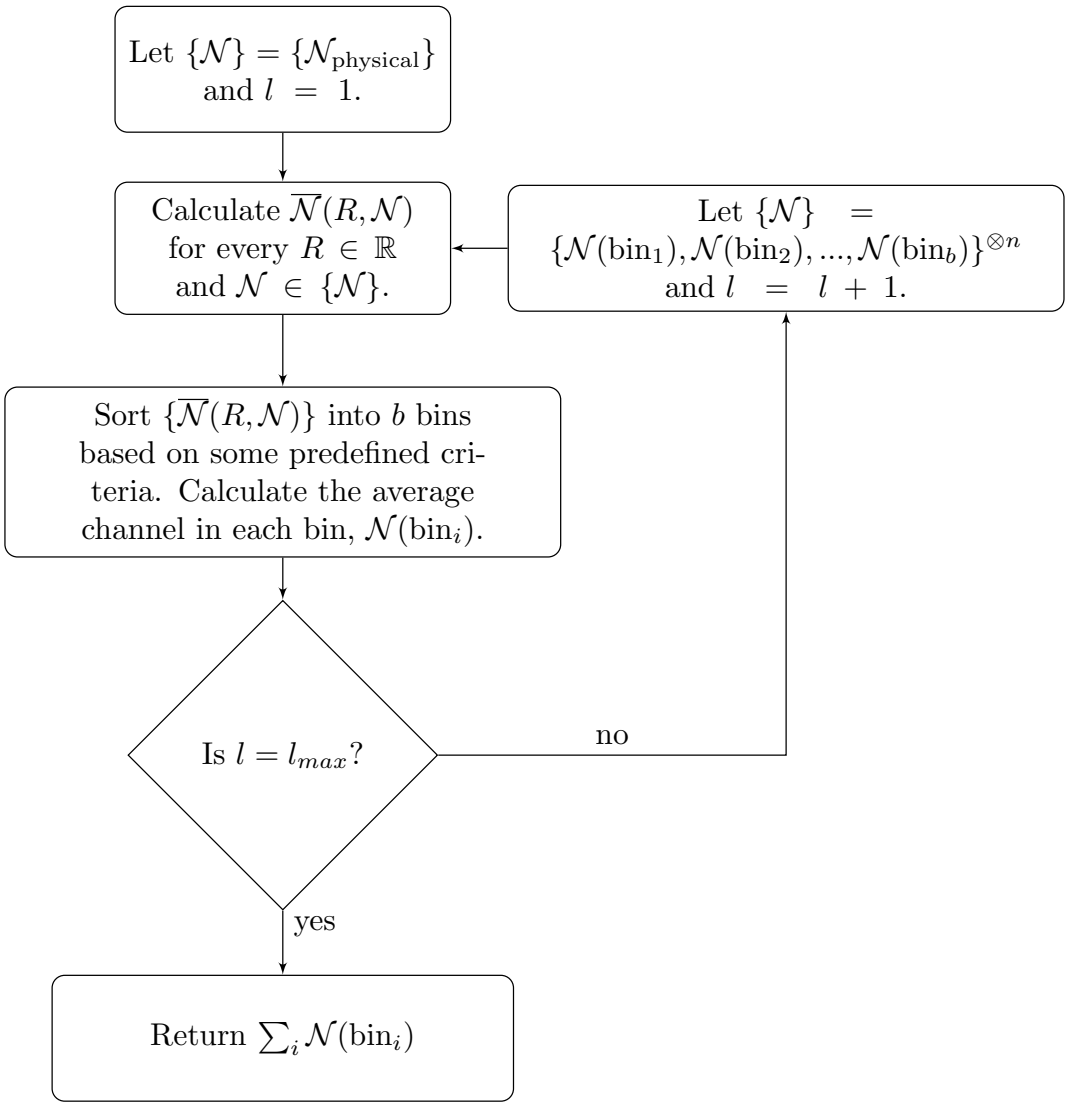

Figure 3.2: An algorithm for soft decoding up to the l_{max}^{th} level in a concatenated code.

examine the effects at the second level of concatenation for different permuatations of trivial and non-trivial noise.

We have already seen that when depolarizing noise acts on the physical qubits in a 5 qubit code as $\mathcal{D}_p^{\otimes 5}$ the resultant noise after symmetric recovery is depolarizing noise with one parameter for the trivial syndrome and a different parameter for the non-trivial syndrome. So when the second level undergoes $\mathcal{N}(\text{bin}_0)^{\otimes 5}$ or $\mathcal{N}(\text{bin}_1)^{\otimes 5}$, it will behave similarly. These two cases correspond to observing the trivial syndrome or a non-trivial syndrome on every code block in the previous level of concatenation. None of these cases exhibits additional symmetry beyond that already observed, so these cases constitute 4 distinct effective channels.

When a permutation of $\mathcal{N}(\text{bin}_0)^{\otimes 4} \otimes \mathcal{N}(\text{bin}_1)$ or $\mathcal{N}(\text{bin}_0) \otimes \mathcal{N}(\text{bin}_1)^{\otimes 4}$ occurs at the first level of concatenation, there are 6 distinct effective channels that can result, and all of them are depolarizing. The first two arise when the trivial syndrome is measured for either of these noises. The remaining four correspond to the cases when the recovery operation acts trivially or non-trivially on the $\mathcal{N}(\text{bin}_i)$ that acts only on one codeblock.

The remaining cases correspond to when the previous codeblocks undergo noise of the form of permutations of $\mathcal{N}(\text{bin}_0)^{\otimes 2} \otimes \mathcal{N}(\text{bin}_1)^{\otimes 3}$ or $\mathcal{N}(\text{bin}_0)^{\otimes 3} \otimes \mathcal{N}(\text{bin}_1)^{\otimes 2}$. These noise models produce depolarizing channels when the trivial syndrome is measured and when the recovery operation acts non-trivially on a codeblock undergoing $\mathcal{N}(\text{bin}_i)$ for noise in the form $\mathcal{N}(\text{bin}_i)^{\otimes 2} \otimes \mathcal{N}(\text{bin}_j)^{\otimes 3}$. These cases form 4 more equivalence classes. The remaining channels are not depolarizing and there are 6 distinct cases.

The recovery protocol we have selected is to apply the typical symmetric recovery to any channels which are depolarizing, and apply the symmetric recovery multiplied by a logical operator when the noise is not depolarizing. The logical operator is selected to maximize the diagonal elements in order to minimize infidelity. This is the same method for selection of recovery for an individual syndrome as that we proposed in [10].

After recovery operations are applied, we sort the effective channels into two categories. This can be implemented in a variety of ways; we partition into bins as follows: We first average over the non-depolarizing channels, grouping them into two sets based on the incoming noise: one set containing permuatations of $\mathcal{N}(\text{bin}_0)^{\otimes 2} \otimes \mathcal{N}(\text{bin}_1)^{\otimes 3}$ and the other set containing permutations of $\mathcal{N}(\text{bin}_0)^{\otimes 3} \otimes \mathcal{N}(\text{bin}_1)^{\otimes 2}$, each of which averages to a depolarizing channel. We then take the ratio of the $\mathcal{N}(\text{bin}_i)_{\sigma,\sigma}$ to the $\mathcal{N}(\text{bin}_i)_{I,I}$, $\sigma \neq I$, and group the corresponding noises into distinct sets based on whether this ratio is larger or smaller than a cutoff. We checked cutoff values between 0 and 1 in increments of 0.01 and the cutoff values that produced the largest threshold value were in $[0.69, 0.73]$, all of which

produced the same threshold. This binning and recovery method results in a threshold value of $p = 0.2348$, which is an improvement over the threshold achieved by hard decoding, $p = 1 - \sqrt{2/3} = 0.1835$.

Another method of binning was considered, in which the cutoff value was set at each level of concatenation to the ratio of $\mathrm{Max}_i\{\mathcal{N}(\mathrm{bin}_i)_{\sigma,\sigma}/\mathcal{N}(\mathrm{bin}_i)_{I,I}\}$ for the input noise from the previous level. This produced a threshold value of $p = 0.2083$.

The threshold value achieved in this section could be improved upon by introducing more bins, partitioning into bins in a different manner, or by doing more than one level of concatenation between coarse graining, e.g by binning after every two levels of error correction. Ref. [12] presented a soft decoding algorithm which achieved a threshold value of $p = 0.2513$. This value was obtained via statistical sampling. While the algorithm we have presented for the 5 qubit code has a slightly lower threshold, the cost to simulate it directly is significantly less, and with the modifications suggested, it is possible that our algorithm could match the algorithm presented in [12].

3.2.4 Depolarizing Noise in the Steane Code

This section explores the behaviour of the effective logical noise resulting from applying depolarizing noise to each physical qubit in a concatenated Steane code when symmetric or CSS recovery operations are applied.

Additional Symmetry in the Steane Code Under Depolarizing Noise

While depolarizing noise is highly symmetric, there is no guarantee that a given stabilizer code will have more equivalent recovery operations when it undergoes depolarizing noise. The Steane code, for example, retains the same equivalence classes for CSS or symmetric recovery under depolarizing noise as under any arbitrary noise model.

Depolarizing Noise Under CSS Recovery in the Steane Code

Applying CSS recovery to a state encoded in the Steane code undergoing depolarizing noise produces an average effective channel of the following form

$$\begin{bmatrix} 1 & 0 & 0 & 0 \\ 0 & \alpha & 0 & 0 \\ 0 & 0 & \beta & 0 \\ 0 & 0 & 0 & \alpha \end{bmatrix}, \tag{3.21}$$

where

$$\alpha = 1 - \frac{21}{2}p^2 + \frac{49}{2}p^3 - \frac{105}{4}p^4 + \frac{63}{4}p^5 - \frac{21}{4}p^6 + \frac{3}{4}p^7 \tag{3.22}$$

and

$$\beta = 1 - \frac{63}{4}p^2 + \frac{91}{2}p^3 - \frac{945}{16}p^4 + \frac{651}{16}p^5 - \frac{231}{16}p^6 + \frac{33}{16}p^7. \tag{3.23}$$

Defining a Pauli channel where X and Z operations are equiprobable,

$$\mathcal{P}[\rho] = (1 - 2p_{xz} - p_y)I\rho I + p_{xz}(X\rho X + Z\rho Z) + p_y Y\rho Y, \tag{3.24}$$

results in a process matrix,

$$\mathcal{P} = \begin{bmatrix} 1 & 0 & 0 & 0 \\ 0 & 1 - 2(p_y + p_{xz}) & 0 & 0 \\ 0 & 0 & 1 - 4p_{xz} & 0 \\ 0 & 0 & 0 & 1 - 2(p_{xz} + p_y) \end{bmatrix}, \tag{3.25}$$

which has a form similar to that of eq. (3.21). Letting $\alpha = 1 - 2(p_y + p_{xz})$ and $\beta = 1 - 4p_{xz}$, it is clear that the average effective logical channel is given by eq. (3.24) with

$$p_{xz} = \frac{1}{64}(252p^2 - 728p^3 + 945p^4 - 651p^5 + 231p^6 - 33p^7) \tag{3.26}$$

and

$$p_y = \frac{1}{64}(84p^2 - 56p^3 - 105p^4 + 147p^5 - 63p^6 + 9p^7). \tag{3.27}$$

Re-encoding Pauli noise of the form eq. (3.24) in the Steane code and applying CSS recovery results in a logical channel with the same form, with

$$\begin{aligned} p_{xz-logical} = & -42p_{xz}^4(-1+2p_{xz})(5+2p_{xz}(-9+10p_{xz})) \\ & + 42(1-2p_{xz})^2p_{xz}^2(5+2p_{xz}(-8+7p_{xz}))p_y \\ & + 21(1-8p_{xz}+24p_{xz}^3(4-9p_{xz}+6p_{xz}^2))p_y^2 \\ & + 14(-7+12p_{xz}(4-7p_{xz}+6p_{xz}^3))p_y^3 \\ & - 42(-1+2p_{xz})(5+6p_{xz}(-3+2p_{xz}))p_y^4 \\ & - 252(1-2p_{xz})^2p_y^5 + 168(1-2p_{xz})p_y^6 - 48p_y^7 \end{aligned} \tag{3.28}$$

and

$$\begin{aligned} p_{y-logical} = & \, p_{xz}(p_{xz}(21-98p_{xz}+12p_{xz}^3(77+2p_{xz}(-91+68p_{xz}))) \\ & - 42(1-2p_{xz})^4(-1+4p_{xz})p_y - 126(-1+2p_{xz})^3(-1+4p_{xz})p_y^2 \\ & - 168(1-2p_{xz})^2(-1+4p_{xz})p_y^3 - 84(1-6p_{xz}+8p_{xz}^2)p_y^4). \end{aligned} \tag{3.29}$$

Then a state encoded in the Steane undergoing depolarizing noise at the physical level will have the form of eq. (3.24) at the l^{th} level of concatenation $\forall l \geq 2$.

Defining a logical error rate for eq. (3.24) of $2p_{xz} + p_y$, and a physical error rate, $3p/4$[9], for depolarizing noise, we plot the logical error rate for the first 4 levels of concatenation as a function of the physical error rate in fig. 3.3[10].

[9] The constant factor is a normalization to allow for a more meaningful comparison between this and the logical error rate.

[10] Note that in this plot the intersection of error rates for consecutive levels of concatenation is not the threshold, but rather a pseudo-threshold, which indicates the value below which the next level will outperform the previous. The pseudo-threshold between the first and second levels of concatenation is larger than the pseudo-thresholds for other consecutive concatenations shown; because the intersections do not all occur at the same value, we cannot ascertain the general threshold value from the intersections. This apparent instability occurs because with multi-parameter noise, the dependencies between the noise parameters between levels is more complex. With infinite concatenation, however, the plot will converge to a step function, for which the vertical asymptote is the threshold value.

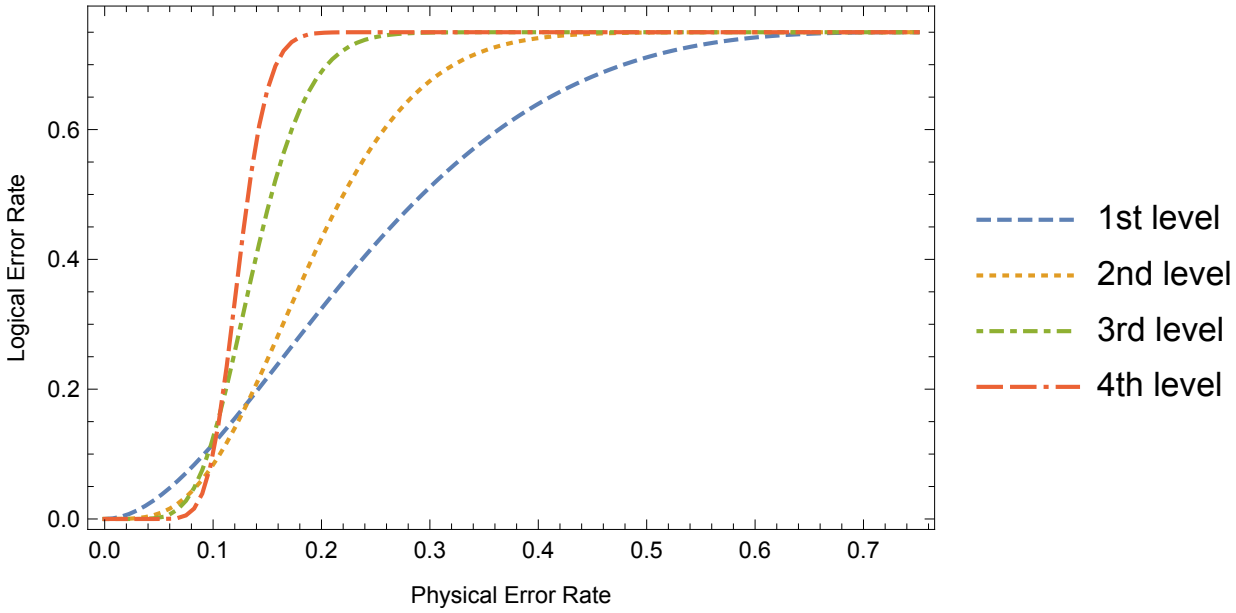

Figure 3.3: Plots of the logical noise rate, defined as $2p_{xz} + p_y$, as a function of the physical depolarizing noise parameter, renormalized to represent a similar error rate.

Depolarizing Noise Under Symmetric Recovery in the Steane Code

Under symmetric decoding, depolarizing noise undergoes a similar evolution with concatenation. At the first level, the effective logical noise is given by eq. (3.21), with

$$\alpha = 1 - 12p^2 + \frac{61}{2}p^3 - \frac{285}{8}p^4 + \frac{183}{8}p^5 - \frac{63}{8}p^6 + \frac{9}{8}p^7, \tag{3.30}$$

and

$$\beta = 1 + 2p - \frac{39}{4}p^2 + 12p^3 - \frac{105}{16}p^4 + \frac{21}{16}p^5. \tag{3.31}$$

Subsequent concatenation preserves the the form of a Pauli channel with equi-probable X and Z errors. The details of this evolution are omitted for brevity.

Chapter 4

Conclusion

In this thesis, we presented a method for approximating the effective logical noise in a quantum error correcting code in terms of the physical infidelity, r, and derived equations for the calculation of process matrices up to a specified order in r. This can significantly reduce the computational complexity of calculating the effective logical noise while preserving most of the accuracy of the full calculation. We gave bounds on the lowest order term in the logical noise in terms of the physical infidelity, and gave qualitative arguments that encoding in a quantum error correcting code and applying syndrome measurements decoheres both local and non-local noise, on average, even without the application of recovery operations. We showed that the decoherence of noise produced by error correction protocols scales with code distance so that, for an arbitrary $[\![n, k, d]\!]$ code, noise should converge to a probabilistic Pauli channel on average as d increases. From these conclusions, we argued that the logical fidelity is a reasonable metric by which the performance of a given set of recovery operations can be assessed. This is useful because, since the logical fidelity is a linear function of quantum channels, we can optimize the logical fidelity per syndrome in order to optimize the total average fidelity when selecting recovery operations, which drastically reduces resource requirements relative to attempting to optimize a metric that is not linear in quantum channels, like the diamond distance.

We proved that in an $[\![n, k, d]\!]$ code, it is impossible for noise acting on fewer than d qubits to produce non-Pauli noise at the logical level.

We presented generalized conditions under which $\overline{\mathcal{N}}(R) = \overline{\mathcal{N}}(R')$ for $R \neq R'$. In sections 3.1.1 to 3.1.3, we presented equivalence classes in popular sets of recovery operators for the 3 qubit repetition code, the 5 qubit code, the Steane code, and the Shor code. We presented additional symmetries that arise when the 5 qubit code undergoes depolarizing

noise, and showed that for the Steane code, depolarizing noise has the same equivalence classes as under general noise for the CSS recovery and a symmetric recovery.

In section 3.2, we derived an expression for the effective logical noise when each physical qubit in the encoding undergoes depolarizing noise, and demonstrated that in the 5 qubit code with symmetric recovery, depolarizing noise on each physical qubit manifests as depolarizing noise at the logical level, with a new noise parameter. From this expression, we calculated the threshold limit. We further showed that in the Steane code, under symmetric or CSS recovery, physical Pauli noise with equi-probable X and Z errors results in logical noise of the same form. After encoding in the Steane code and applying CSS or symmetric recovery, depolarizing noise manifests as Pauli noise with equi-probable X and Z errors. We also presented a general expression for Pauli noise in a quantum error correcting code.

We proposed a soft decoding algorithm which can be exactly simulated and thus does not rely on statistical sampling methods, and applied it to the 5 qubit code, demonstrating an improvement over hard decoding techniques. This algorithm was presented in its general form, and future research will include exploring the effects of changing methods for binning noise at each level of concatenation, how many levels of concatenation are implemented between binning, and how many bins are used. The algorithm will also be used for other quantum error correcting codes and noise.

References

[1] Robert E. Fontana Jr. and Gary M. Decad. Moores law realities for recording systems and memory storage components: Hdd, tape, nand, and optical. *AIP Advances*, 8:056506, 2018.

[2] Richard P. Feynman. Simulating physics with computers. *International Journal of Theoretical Physics*, 21:467-488, 1982.

[3] Christian Dickel. Programming for the quantum computer. *Qutech: Bits of Quantum*, 2016.

[4] Joel Wallman, Chris Granade, Robin Harper, and Steven T. Flammia. Estimating the coherence of noise. *New Journal of Physics*, 17:113020, 2015.

[5] Easwar Magesan. Gaining Information About a Quantum Channel Via Twirling. *uwspace.uwaterloo.ca*, 2008.

[6] Leonardo Bautista-Gomez, Ferad Zyulkyarov, Osman Unsal, and Simon McIntosh-Smith. Unprotected computing: A large-scale study of dram raw error rate on a supercomputer. *SC '16: Proceedings of the International Conference for High Performance Computing, Networking, Storage and Analysis*, 2167-4337, 2016.

[7] William K. Wootters and Wojciech H Zurek. A single quantum cannot be cloned. *Nature*, 299:802-803, 1982.

[8] Emanuel Knill and Raymond Laflamme. Theory of quantum error-correcting codes. *Physical Review A*, 55:900, 1997.

[9] Daniel Gottesman. Surviving as a quantum computer in a classical world. *Textbook manuscript preprint*, 2016.

[10] Christopher Chamberland, Joel J. Wallman, Stefanie Beale, and Raymond Laflamme. Hard decoding algorithm for optimizing thresholds under general Markovian noise. *Physical Review A*, 95:042332, 2017.

[11] David Poulin. Tensor networks and quantum error correction. *Physical Review Letters*, 113:030501, 2014.

[12] David Poulin. Optimal and efficient decoding of concatenated quantum block codes. *Physical Review A*, 74:052333, 2006.

[13] Tomas Jochym-O'Connor and Raymond Laflamme. Using concatenated quantum codes for universal fault-tolerant quantum gates. *Physical Review Letters*, 112:010505, 2014.

[14] Stefan M. Moser and Po-Ning Chen. A student's guide to coding and information theory. *Cambridge*, 2012.

[15] Christopher Chamberland and Pooya Ronagh. Deep neural decoders for near term fault-tolerant experiments. *Arxiv preprint*, 1802.06441, 2018.

[16] Jesse Fern. Correctable noise of quantum-error-correcting codes under adaptive concatenation. *Physical Review A*, 77:010301, 2008.

[17] Joseph Emerson, Robert Alicki, and Karol Życzkowski. Scalable noise estimation with random unitary operators. *Journal of Optics B*, 7:S347, 2005.

[18] Michael A. Nielsen. A simple formula for the average gate fidelity of a quantum dynamical operation. *Physics Letters A*, 303:249252, 2002.

[19] Joel J. Wallman and Steven T. Flammia. Randomized benchmarking with confidence. *New Journal of Physics*, 16:103032, 2014.

[20] Salman Beigi and Robert König. Simplified instantaneous non-local quantum computation with applications to position-based cryptography. *New Journal of Physics*, 13:125202, 2011.

[21] Yuval R Sanders, Joel J. Wallman, and Barry C. Sanders. Bounding quantum gate error rate based on reported average fidelity. *New Journal of Physics*, 18:012002, 2015.

[22] Richard Keung, David M. Long, Andrew Doherty, and Steven T. Flammia. Comparing experiments to the fault-tolerance threshold. *Physical Review Letters*, 117:170502, 2016.

[23] I. Pavithran and D. Poulin. A small quantum computer is needed to optimize fault-tolerant protocols. *arXiv preprint*, 1711.04736, 2017.

[24] J. S. Otterbach, R. Manenti, N. Alidoust, A. Bestwick, M. Block, B. Bloom, S. Caldwell, N. Didier, E. Schuyler Fried, S. Hong, P. Karalekas, C. B. Osborn, A. Papageorge, E. C. Peterson, G. Prawiroatmodjo, N. Rubin, Colm A. Ryan, D. Scarabelli, M. Scheer, E. A. Sete, P. Sivarajah, Robert S. Smith, A. Staley, N. Tezak, W. J. Zeng, A. Hudson, Blake R. Johnson, M. Reagor, M. P. da Silva, and C. Rigetti. Unsupervised machine learning on a hybrid quantum computer. *arXiv preprint*, 1712.05771, 2017.

[25] Nicolai Friis, Oliver Marty, Christine Maier, Cornelius Hempel, Milan Holzapfel, Petar Jurcevic, Martin B. Plenio, Marcus Huber, Christian Roos, Rainer Blatt, , and Ben Lanyon. Observation of Entangled States of a Fully Controlled 20-Qubit System. *Physical Review X*, 8: 021012, 2018.

[26] IBM Quantum Experience. *IBM Q*, Web, 2018.

[27] Intel Delivers 17-Qubit Superconducting Chip with Advanced Packaging to QuTech. *Intel News Byte*, Web, 2017.

[28] 2018 CES: Intel Advances Quantum and Neuromorphic Computing Research. *Intel News Byte*, Web, 2018.

[29] J. Kelly, R. Barends, A. G. Fowler, A. Megrant, E. Jeffrey, T. C. White, D. Sank, J. Y. Mutus, B. Campbell, Yu Chen, Z. Chen, B. Chiaro, A. Dunsworth, I.-C. Hoi, C. Neill, P. J. J. OMalley, C. Quintana, P. Roushan, A. Vainsencher, J. Wenner, A. N. Cleland, and John M. Martinis. State preservation by repetitive error detection in a superconducting quantum circuit. *Nature*, 519: 6669, 2015.

[30] S. Debnath, N. M. Linke, C. Figgatt, K. A. Landsman, K. Wright, and C. Monroe. Demonstration of a small programmable quantum computer with atomic qubits. *Nature*, 536: 6366, 2016.

[31] Julian Kelly. A Preview of Bristlecone, Google's New Quantum Processor. *Google AI Blog*, Web, 2018.

[32] Chad Rigetti. The Rigetti 128-qubit chip and what it means for quantum. *Medium*, Web, 2018.

[33] Benjamin Rahn, Andrew C. Doherty, and Hideo Mabuchi. Exact performance of concatenated quantum codes. *Physical Review A*, 66:032304, 2002.

[34] Jesse Fern, Julia Kempe, Slobodan Simic, and S. Sastry. Generalized Performance of Concatenated Quantum Codes: A Dynamical Systems Approach. *IEEE Transactions on Automatic Control*, 51:448, 2006.

[35] Stefanie Beale, Joel Wallman, Mauricio Guiérrez, Kenneth R. Brown, and Raymond Laflamme. Coherence in quantum error correcting codes. *arXiv preprint*, 1805.08802, 2018.

[36] C. King and M. B. Ruskai. Minimal entropy of states emerging from noisy quantum channels. *IEEE Transactions on Information Theory*, 47:192-209, 2001.

[37] Mary Beth Ruskai, Stanislaw Szarek, and Elisabeth Werner. An analysis of completely positive trace-preserving maps on $\mathcal{M}_2$. *Linear Algebra and its Applications*, 347:159-187, 2002.

[38] Mauricio Gutiérrez, Conor Smith, Livia Lulushi, Smitha Janardan, and Kenneth R. Brown. Errors and pseudothresholds for incoherent and coherent noise. *Physical Review A*, 94:042338, 2016.

[39] Eric Huang, Andrew C. Doherty, and Steven Flammia. Performance of quantum error correction with coherent errors. *Arxiv preprint*, 1805.08227, 2018.

[40] Paul Henry Seagraves. Representation of permutation operators in quantum machanics. *BSc. Thesis, New Mexico Institute of Mining and Technology*, 1963.

Appendix A

Derivation of eq. (1.70)

Recall from eq. (1.31), in the Pauli basis,

$$|\rho\rangle\rangle = \sum_{\sigma} \mathrm{Tr}(B_\sigma^\dagger \rho) e_\sigma, \tag{A.1}$$

where $\{e_\sigma\}$ is the canonical basis. Then,

$$\langle\langle (S\overline{\sigma})_j | \mathcal{N}^{(j)} | (S'\overline{\sigma}')_j \rangle\rangle = \sum_{\tau,\zeta\in\mathbb{P}} \mathrm{Tr}[(S\overline{\sigma})_j^\dagger B_\tau] e_\tau^\dagger \mathcal{N}^{(j)} \mathrm{Tr}[B_\zeta^\dagger (S'\overline{\sigma}')_j] e_\zeta \tag{A.2}$$

$$= \sum_{\tau,\zeta\in\mathbb{P}} \mathrm{Tr}[(S\overline{\sigma})_j^\dagger B_\tau] \mathrm{Tr}[B_\zeta^\dagger (S'\overline{\sigma}')_j] \mathcal{N}^{(j)}_{\tau,\zeta}. \tag{A.3}$$

We define an operator $H = \chi(H)J$, where $J \in \mathbb{P}$, and $\chi(H)$ is a constant. Then $\mathrm{Tr}[B_\zeta^\dagger H] = \frac{2}{\sqrt{2}}\chi(H)\delta_{\zeta,J}$, where the factor of $1/\sqrt{2}$ comes from the normalization of B_ζ. Equation (A.3) can then be simplified as

$$\langle\langle (S\overline{\sigma})_j | \mathcal{N}^{(j)} | (S'\overline{\sigma}')_j \rangle\rangle = 2\chi((S\overline{\sigma})_j)\chi((S'\overline{\sigma}')_j) \mathcal{N}^{(j)}_{(S\overline{\sigma})_j,(S'\overline{\sigma}')_j} \tag{A.4}$$

where we have generalized the definition of $\chi(\cdot)$ to be the phase on the input Pauli operator relative to the Pauli group. Extending this further so that $\chi(\cdot)$ can be the phase on an operator relative the the n-qubit Pauli group,

$$\langle\langle S\overline{\sigma}|\mathcal{N}|S'\overline{\sigma}'\rangle\rangle = \bigotimes_{j\in\mathbb{Z}_n} \langle\langle (S\overline{\sigma})_j|\mathcal{N}^{(j)}|(S'\overline{\sigma}')_j\rangle\rangle \tag{A.5}$$

$$= \bigotimes_{j\in\mathbb{Z}_n} 2\chi((S\overline{\sigma})_j)\chi((S'\overline{\sigma}')_j)\mathcal{N}^{(j)}_{(S\overline{\sigma})_j,(S'\overline{\sigma}')_j} \tag{A.6}$$

$$= 2^n\chi(S\overline{\sigma})\chi(S'\overline{\sigma}') \prod_{j\in\mathbb{Z}_n} \mathcal{N}^{(j)}_{(S\overline{\sigma})_j,(S'\overline{\sigma}')_j}. \tag{A.7}$$

Appendix B

Equivalence Classes for Symmetric Recovery in the Shor Code

The partitioning of a set of symmetric recovery operations for the Shor code into equivalence classes by $(4\,7)(5\,8)(6\,9)$ and $(1\,4)(2\,5)(3\,6)(7\,8\,9)$ is given in table B.1.

Class	Recovery Operators
1	$I^{\otimes 7}$
2	$IIIIIIIZ$, $IIIZIIII$, $ZIIIIIII$
3	$IIIIXIII$, $IIIIIXII$, $IIIIIIIX$, $IIXIIIII$, $IIIXIIII$, $IIIIIIXI$, $XIIIIIII$, $IIIIXIII$, $IXIIIIII$
4	$IIIIIYII$, $IIIIIIYI$, $IIIIIIIY$, $IIYIIIII$, $IIIYIIII$, $IIIIIIYI$, $YIIIIIII$, $IIIIYIII$, $IYIIIIII$
5	$ZIIIIXII$, $IIIZIIXI$, $ZIIIIIIX$, $IIXZIIII$, $ZIIIIIXI$, $ZIIIXIII$, $IIIZIIIX$, $IXIZIIII$, $ZIIIIIXI$, $IIXIIIIZ$, $ZIIXIIII$, $IIIZIIXI$, $XIIZIIII$, $IIIIXIIZ$, $IXIIIIIZ$, $IIIIXIIZ$
6	$IIIIIXIIX$, $IIXIIIXI$, $IIXXIIII$, $IIIIIXIXI$, $XIIIIXIII$, $IIIIXIIIX$, $IIXIIIIX$, $XIIIIIIX$, $IXIIIIXII$, $IIXIIXIII$, $IIIIIXXII$, $IIIXIIXII$, $IXIXIIII$, $IIIIXIIXI$, $IIIXIIIIX$, $IIXIIIIXI$, $XIIIIIIXI$, $XIIIXIII$, $IXIIIIIX$, $XIIIIIXII$, $IIXIXIII$, $IXIIIXIII$, $IIIIXIXII$, $XIIXIIII$, $IIIXIIIXI$, $IXIIIIIXI$, $IXIIXIII$
7	$IIIIIYIIX$, $IIXIIIYII$, $IIIIIXIIY$, $IIYIIIXII$, $IIXYIIII$, $IIIIIXIYI$, $IIYXIIII$, $IIIIIYIXI$, $YIIIIXIII$, $IIIIYIIIX$,

	$IIXIIIIIY$, $XIIIIYIII$, $IIIIXIIIY$, $IIYIIIIIX$, $YIIIIIIIX$, $IYIIIIXII$, $IIXIIYIII$, $IIIIIXYII$, $XIIIIIIIY$, $IXIIIIYII$, $IIYIIXIII$, $IIIIIYXII$, $IIIYIIXII$, $IYIXIIIII$, $IIIIYIIXI$, $IIIYIIIIX$, $IIXIIIIYI$, $IIIXIIYII$, $IXIYIIIII$, $IIIIXIIYI$, $IIIXIIIIY$, $IIYIIIIXI$, $YIIIIIIXI$, $XIIIYIIII$, $IYIIIIIIX$, $YIIIIIXII$, $IIXIYIIII$, $XIIIIIIYI$, $YIIIXIIII$, $IXIIIIIIY$, $XIIIIIYII$, $IIYIXIIII$, $IYIIIXIII$, $IIIIYIXII$, $YIIXIIIII$, $IIIYIIIXI$, $IXIIIYIII$, $IIIIXIYII$, $XIIYIIIII$, $IIIXIIIYI$, $IYIIIIIXI$, $IXIIIIIYI$, $IYIIXIIII$, $IXIIYIIII$
8	$IIIIIYIIY$, $IIYIIIYII$, $IIYYIIIII$, $IIIIIYIYI$, $YIIIIYIII$, $IIIIYIIIY$, $IIYIIIIIY$, $YIIIIIIIY$, $IYIIIIYII$, $IIYIIYIII$, $IIIIIYYII$, $IIIYIIYII$, $IYIYIIIII$, $IIIIYIIYI$, $IIIYIIIIY$, $IIYIIIIYI$, $YIIIIIIYI$, $YIIIYIIII$, $IYIIIIIIY$, $YIIIIIYII$, $IIYIYIIII$, $IYIIIYIII$, $IIIIYIYII$, $YIIYIIIII$, $IIIYIIIYI$, $IYIIIIIYI$, $IYIIYIIII$
9	$YIIZIIIII$, $ZIIYIIIII$
10	$IIXIIXIIX$, $IIXIIXXII$, $IIXXIIIIX$, $IIXIIXIXI$, $XIIIIXXII$, $IIXIXIIIX$, $XIIXIIIIX$, $IIXXIIIXI$, $IXIIIXXII$, $XIIXIIXII$, $IIXIXIXII$, $XIIIIXIIX$, $IXIXIIIIX$, $IIXIXIIXI$, $XIIXIIIXI$, $IXIIIXIXI$, $IIXXIIXII$, $XIIIXIXII$, $IXIIIXIIX$, $IXIIXIIIX$, $XIIIIXIXI$, $IXIXIIIXI$, $IXIIXIXII$, $XIIIXIIIX$, $IXIIXIIXI$, $IXIXIIXII$, $XIIIXIIXI$
11	$IIXIIYIIX$, $IIXIIXYII$, $IIXIIXIIY$, $IIYIIXXII$, $IIXYIIIIX$, $IIXIIXIYI$, $IIXIIYIXI$, $YIIIIXXII$, $IIXIYIIIX$, $IIXIXIIIY$, $IIYIIXIIX$, $YIIXIIIIX$, $IIXYIIIXI$, $IYIIIXXII$, $IXIIIXYII$, $IIXIIYXII$, $XIIYIIXII$, $IIXIXIYII$, $YIIIIXIIX$, $IIXIYIIXI$, $IIYIXIXII$, $IXIYIIIIX$, $IIXIXIIYI$, $IIXXIIIIY$, $IIYIIXIXI$, $YIIXIIIXI$, $IXIIIXIYI$, $IIXYIIXII$, $IYIIIXIIX$, $IXIIIYIXI$, $XIIIIXIIY$, $YIIIXIXII$, $IXIIIXIIY$, $XIIIIXYII$, $IIYIXIIIX$, $XIIYIIIIX$, $IXIIYIIIX$, $IIXXIIYII$, $YIIIIXIXI$, $IIXIYIXII$, $IXIIXIIIY$, $IXIYIIIXI$, $IXIIIYIIX$, $IIXXIIIYI$, $IXIIIYXII$, $YIIXIIXII$, $IYIIXIXII$, $XIIIIXIYI$, $YIIIXIIIX$, $IYIIIXIXI$, $IXIIXIIIY$, $XIIIXIIIY$, $IXIXIIIIY$, $IIYIXIIXI$, $XIIYIIIXI$, $IXIIYIIXI$, $IXIYIIXII$, $IYIIXIIIX$, $IXIIXIIYI$, $IXIXIIIYII$, $XIIIXIYII$, $YIIIXIIXI$, $IXIIYIXII$, $XIIIXIIYI$, $IXIXIIIYI$,

	$IYIIXIIXI$
12	$YIIIIXYII$, $IIXYIIIIY$, $YIIYIIIIX$, $IIXYIIIYI$, $YIIYIIXII$, $YIIIIXIIY$, $YIIYIIIXI$, $IIXYIIYII$, $YIIIXIYII$, $YIIIIXIYI$, $IXIYIIIYI$, $YIIIXIIIY$, $IXIYIIYII$, $YIIIXIIYI$, $IXIYIIIIY$

Table B.1: Equivalence classes for a symmetric decoder in the 7 qubit Steane code.